

Elevated pyramidal cell firing orchestrates arteriolar vasoconstriction through COX-2-derived prostaglandin E2 signaling

Benjamin Le Gac¹, Marine Tournissac², Esther Belzic¹, Sandrine Picaud¹, Isabelle Dusart¹, Hédi Soula³, Dongdong Li¹, Serge Charpak², Bruno Cauli^{1*}

1. Sorbonne Université, CNRS, INSERM, Institut de Biologie Paris Seine (IBPS), Center for Neuroscience at Sorbonne Université (NeuroSU), 75005, Paris, France, 7 quai Saint Bernard, 75005 Paris, France.

2. Sorbonne Université, INSERM, CNRS, Institut de la Vision, 17 rue Moreau, 75012 Paris, France.

3. Sorbonne Université, INSERM, Nutrition and Obesities: Systemic Approaches, NutriOmics, research unit, 91 boulevard de l'hôpital, 75013 Paris, France.

*Correspondance: bruno.cauli@upmc.fr

Keywords: Neurovascular coupling, pyramidal cells, prostaglandin E2 signaling, optogenetics

1 **Abstract**

2 Neurovascular coupling, linking neuronal activity to cerebral blood flow, is essential for brain
3 function and underpins functional brain imaging. Whereas mechanisms involved in
4 vasodilation are well-documented, those controlling vasoconstriction remain overlooked. This
5 study unravels the mechanisms by which pyramidal cells elicit arteriole vasoconstriction. Using
6 patch-clamp recording, vascular and Ca^{2+} imaging in mouse cortical slices, we show that strong
7 optogenetic activation of layer II/III pyramidal cells induces vasoconstriction, correlating with
8 firing frequency and somatic Ca^{2+} increase. *Ex vivo* and *in vivo* pharmacological investigations
9 indicate that this vasoconstriction predominantly recruits prostaglandin E2 through the
10 cyclooxygenase-2 pathway, and activation of EP1 and EP3 receptors. We also present evidence
11 that specific interneurons releasing neuropeptide Y, and astrocytes, through 20-
12 hydroxyeicosatetraenoic acid, contribute to this process. By revealing the mechanisms by
13 which pyramidal cells lead to vasoconstriction, our findings shed light on the complex
14 regulation of neurovascular coupling.

15 **Significance statement**

16 Cerebral blood flow is tightly controlled by neuronal activity, a process termed neurovascular
17 coupling which serves as the physiological basis for functional brain imaging widely used to
18 map neuronal activity in health and diseases. While the prevailing view links increased
19 neuronal activity with enhanced blood perfusion, our data suggest that elevated neuronal
20 activity can also reduce cerebral blood flow. By optically controlling the activity of pyramidal
21 cells, we demonstrate that these excitatory neurons induce vasoconstriction when their action
22 potential firing is increased by releasing glutamate and lipid messengers. These findings
23 update the interpretation of functional brain imaging signals and help to better understand
24 the etiopathogenesis of epilepsy and Alzheimer's disease, in which hyperactivity,
25 hypoperfusion and cognitive deficits overlap.

26 Introduction

27 The brain critically depends on the uninterrupted blood supply provided by a dense
28 vasculature (Schmid et al., 2019). Cerebral blood flow (CBF) is locally and temporally controlled
29 by neuronal activity, by an essential process called neurovascular coupling (NVC), and is
30 impaired in early stages of numerous neurological disorders (Iadecola, 2017). NVC also serves
31 as the physiological basis for functional brain imaging widely used to map neuronal activity.
32 Neuronal activity increases CBF within seconds (Iadecola, 2017). In the cerebral cortex, the
33 hyperemic response linked to neural activity is supported by dynamically controlled
34 vasodilation that is spatially and temporally constrained by vasoconstriction in a second phase
35 (Devor et al., 2007). Conversely, vasoconstriction and decreased CBF usually correlate with
36 reduced neuronal activity (Devor et al., 2007; Shmuel et al., 2002).

37 Mounting evidence indicates that the positive correlation between neuronal activity and CBF
38 is not always maintained under physiological conditions: i) robust sensory-evoked vasodilation
39 can occur in the absence of substantial neuronal response (O'Herron et al., 2016), ii)
40 conversely, pronounced neuronal activity is not systematically associated with increased
41 hemodynamics (Ma et al., 2016), iii) CBF is decreased in several cortical areas despite local
42 increase in neuronal activity (Devor et al., 2008), and iv) optogenetic simulation of inhibitory
43 GABAergic interneurons results in vasodilation (Uhlirova et al., 2016). Furthermore, in
44 pathological conditions with intense neuronal activity such as epileptic seizures, a sustained
45 hypoperfusion induced by vasoconstriction is observed (Farrell et al., 2016; Tran et al., 2020).

46 NVC is achieved by the synthesis and release of vasoactive messengers within the
47 neurovascular unit (Iadecola, 2017), which act on the contractility of mural cells (smooth
48 muscle cells and pericytes) to control vessel caliber and CBF along the vascular tree (Rungta et
49 al., 2018). Pial and penetrating arterioles, which have a higher density of contractile mural cells
50 and control their diameter faster than capillaries (Hartmann et al., 2021; Hill et al., 2015;
51 Rungta et al., 2021, 2018), play a key role in regulating CBF.

52 Different experimental approaches, each with their advantages and limitations, have allowed
53 the identification of several mediators of NVC (Grutzendler and Nedergaard, 2019; Iadecola
54 and Nedergaard, 2007). *Ex vivo* brain slices provide a well-controlled environment, ideal for
55 pharmacological investigations to dissect the underlying mechanisms. However, they lack

56 connectivity and blood flow which provides both vascular tone and natural oxygenation and
57 therefore require *in vivo* validation. Conversely, pharmacological studies are more challenging
58 with *in vivo* preparations. Awake animals allow physiologically relevant context with largely
59 undisturbed network and neuromodulatory activity. However, this preparation is subject to
60 brain state changes which may affect network activity, metabolism, and vascular physiology
61 (Grutzendler and Nedergaard, 2019), potentially complexifying the analysis of specific
62 mechanisms of NVC. Although chronic anesthetized animals have reduced network and
63 neuromodulation activity, the NVC response is only slowed (Rungta et al., 2021), providing a
64 valuable model for validating *ex vivo* observations.

65 Messengers of vasodilation released by excitatory neurons, GABAergic interneurons,
66 astrocytes, or endothelial cells, include nitric oxide, K^+ , arachidonic acid derivatives such as
67 prostaglandin E2 (PGE2) (Iadecola, 2017), or more recently glutamate (Zhang et al., 2024).
68 Despite its physio pathological importance, vasoconstriction is less understood with fewer cell
69 types and vasoactive messengers that have been identified. It is now generally accepted that
70 GABAergic interneurons are key players in vasoconstriction by releasing neuropeptide Y (NPY)
71 (Cauli et al., 2004; Uhlirova et al., 2016). Under certain conditions, astrocytes can also induce
72 vasoconstriction via 20-hydroxyeicosatetraenoic acid (20-HETE) (Mulligan and MacVicar, 2004)
73 or high K^+ concentration (Girouard et al., 2010). However, the involvement of pyramidal cells
74 in vasoconstriction has been overlooked.

75 PGE2 has emerged as a bimodal messenger of NVC, similar to K^+ (Girouard et al., 2010) and
76 glutamate (Zhang et al., 2024), that can induce either vasodilation (Gordon et al., 2008; Lacroix
77 et al., 2015; Lecrux et al., 2011; Mishra et al., 2016) or vasoconstriction (Dabertrand et al.,
78 2013; Rosehart et al., 2021) depending on its concentration and/or site of action along the
79 vascular tree. Under physiological conditions, PGE2 is produced during NVC by either
80 astrocytes (Mishra et al., 2016) or pyramidal cells (Lacroix et al., 2015) via the rate-limiting
81 synthesizing enzymes cyclooxygenase-1 (COX-1) or -2 (COX-2), respectively. Since COX-2-
82 expressing pyramidal cells can release glutamate and PGE2, both of which induce
83 vasoconstriction at high concentrations (Dabertrand et al., 2013; Rosehart et al., 2021; Zhang
84 et al., 2024), pyramidal cells may be responsible for vasoconstriction when their spiking
85 activity is high.

86 To test this hypothesis, we used *ex vivo* and *in vivo* approaches in combination with
87 optogenetics to precisely control pyramidal cell firing in the mouse barrel cortex while
88 monitoring the resulting arteriolar response. We found that pyramidal cells induce
89 vasoconstriction at high stimulation frequency and about half of them express all the
90 transcripts required for a cell autonomous synthesis of the vasoconstrictor messengers PGE2
91 and prostaglandin F2 α (PGF2 α). Pharmacological investigations revealed that this neurogenic
92 vasoconstriction depends on COX-2-derived PGE2 via the direct activation of vascular EP1 and
93 EP3 receptors. It also involves the recruitment of intermediary NPY interneurons acting on the
94 Y1 receptor, and, to a lesser extent astrocytes, via 20-HETE and COX-1-derived PGE2. Thus, our
95 study reveals the mechanisms by which high frequency pyramidal cell firing leads to
96 vasoconstriction.

97 Results

98 Pyramidal cells induce vasoconstriction at high firing frequency.

99 To determine if pyramidal cells action potential (AP) firing can induce vasoconstriction in a
100 frequency-dependent manner, we used optogenetics to induce AP firing while monitoring the
101 resulting vascular response in cortical slices. We used *Emx1-cre;Ai32* transgenic mice
102 expressing the H134R variant of channelrhodopsin-2 (ChR2) in the cortical glutamatergic
103 neurons (Gorski et al., 2002), conferring robust pyramidal cell photoexcitability (Madisen et
104 al., 2012). Wide-field photostimulation of cortical slices was achieved in layers I to III
105 (Supplementary Fig. 1a) using 10-second trains of 5 ms light pulses (see Methods) delivered at
106 five different frequencies (1, 2, 5, 10 and 20 Hz, Fig. 1a).

107 First, we ensured the efficiency of the photostimulation paradigm by recording layer II-III
108 pyramidal cells in whole-cell current clamp mode (Fig. 1a). We observed that optogenetic
109 stimulation resulted in the firing of an initial AP that was followed by a train of spikes whose
110 amplitude and frequency transiently decreased before reaching a steady state (Fig. 1a, upper
111 traces). Consistent with the kinetic properties of the H134R ChR2 variant (Lin et al., 2009) and
112 the intrinsic firing properties of pyramidal cells (Karagiannis et al., 2009), the steady-state
113 firing frequency matched the photostimulation frequency up to 5 Hz but was lower at higher
114 frequencies (Fig. 1a, steady-state spike success rate: $100 \pm 0\%$ at 1, 2 and 5 Hz, $70 \pm 11\%$ at
115 10 Hz and $55 \pm 12\%$ at 20 Hz). These observations demonstrate efficient pyramidal cell
116 activation over a wide range of photostimulation frequencies.

117 To test the hypothesis that neuronal activity induces vasoconstriction, we analyzed the
118 optogenetically induced response of penetrating arterioles. Layer I arterioles were imaged for
119 30 minutes in cortical slices (Supplementary Fig.2; Supp. table 1) without precontraction to
120 facilitate observation of vasoconstriction (Cauli et al., 2004). Examination of the evoked
121 vascular response over 30-minutes (Supplementary Fig.2) showed that increasing the
122 frequency of photostimulation shifted the overall vascular response from a barely discernible
123 delayed response between 1 Hz and 5 Hz to a sustained vasoconstriction at 10 Hz and above
124 which began less than 2 minutes after photostimulation (10 Hz: 1.4 ± 0.4 min; 20 Hz: 1.6 ± 0.5
125 min). Most vessels ($n=8$ of 10 arterioles) showed a strong and rapid vasoconstriction at 20 Hz.
126 On average, this response peaked at 6.8 ± 2.4 min, much earlier than at lower frequencies,

127 which typically required more than 10 min to reach a maximum (Supplementary Fig.2c, 1 Hz:
128 15.6 ± 4.0 min; 2 Hz: 13.2 ± 2.3 min; 5 Hz: 16.0 ± 3.6 min; 10 Hz: 15.7 ± 2.4 min). Because the
129 vascular response shifted to reliable vasoconstriction, with onset and peak in less than 2 and
130 10 minutes, respectively, similar to previous observations in cortical slices (Cauli et al., 2004),
131 when the frequency of photostimulation was increased to 20 Hz, we defined the first 10
132 minutes of recording as the vasoconstriction time frame for subsequent comparisons and
133 analyses. While photostimulation at 1 to 5 Hz failed to elicit fast reliable vascular responses
134 (Fig. 1c-d), 10 Hz photostimulation predominantly induced vasoconstriction (n= 4 of 5
135 arterioles, Fig. 1 c-d, area under the curve (AUC)= $-1.7 \pm 1.1 \times 10^3$ %·s, n= 5). This response was
136 even more pronounced at 20 Hz, as all arterioles showed vasoconstriction of high magnitude
137 (Fig. 1 b-d; AUC= $-3.7 \pm 0.7 \times 10^3$ %·s, $F_{(4, 30)} = 6.135$, $p = 9.89 \times 10^{-4}$, one-way ANOVA, n= 10
138 arterioles). This difference was particularly striking when comparing the magnitude at 20 Hz
139 (Fig. 1d) with those at 1 Hz ($t_{(12)} = -3.48$, $p = 0.0407$, t-test), 2 Hz ($t_{(18)} = -4.09$, $p = 0.0250$, t-test)
140 and 5 Hz ($t_{(14)} = -3.7$, $p = 0.0346$, t-test). Intense optogenetic stimulation of pyramidal cells has
141 been shown to elicit cortical spreading depression (Chung et al., 2018; Pham et al., 2024),
142 which induces vasoconstriction (Zhang et al., 2024) and fast cell swelling (Zhou et al., 2010).
143 We ruled out this possibility by showing that the rate of change in light transmittance
144 associated with cell swelling remained below that of cortical spreading depression (Zhou et al.,
145 2010) (Supplementary Table 1). On the other hand, ChR2-independent vascular changes
146 induced by high light intensity have been reported (Rungta et al., 2017). We verified that 20
147 Hz photostimulation did not induce a vascular response in wild-type mice that do not express
148 ChR2 (Supplementary Fig.1). Taken together, our observations indicate that photostimulation
149 of pyramidal cells produces a frequency-dependent vasoconstriction.

150 **Optogenetic stimulation induces a frequency-dependent, gradual increase in somatic**
151 **calcium that precedes the vascular response.**

152 These observations raise the questions of how pyramidal neurons can induce vasoconstriction
153 at higher AP-firing rates. It is generally accepted that the synthesis and/or release of
154 vasodilatory substances requires an increase in intracellular Ca^{2+} in the releasing cells (Attwell
155 et al., 2010; Cauli and Hamel, 2010), but little is known about the release of vasoconstricting
156 substances. We therefore determined whether an increase in somatic Ca^{2+} concentration in
157 cortical neurons was also dependent on photostimulation frequency. We combined

158 optogenetic stimulation with whole-cell current clamp recording and intracellular Ca²⁺
159 imaging using Rhod-2 delivered by patch pipette (Fig. 2a). Excitation of this red Ca²⁺ indicator
160 at 585 nm did not induce any voltage response in the recorded pyramidal cells (Fig. 2a), as
161 expected from the action spectrum of ChR2(Lin et al., 2009). In contrast, photostimulation at
162 470 nm elicited a train of spikes accompanied by a somatic Ca²⁺ increase that decayed for tens
163 of seconds after photostimulation without triggering any significant recurrent spiking activity
164 (Supplementary Fig. 3). The Ca²⁺ response evoked by 20 Hz photostimulation was more than
165 twice of that evoked by 2 Hz photostimulation (Fig. 2b; 2 Hz: $\Delta F/F_0 = 34.5 \pm 3.7\%$, n= 9 cells,
166 vs. 20 Hz: $\Delta F/F_0 = 79.5 \pm 17.7\%$, n= 9 cells; $t_{(16)} = 2.485$, p= 0.024397), while the average number
167 of evoked spikes was about five times higher (Fig. 1a and supplementary Fig. 3). These results
168 demonstrate a frequency-dependent increase in intracellular Ca²⁺ induced by
169 photostimulation, that precedes vasoconstriction. We therefore aimed to understand the
170 molecular mechanisms linking neuronal activity to vasoconstriction.

171 **Vasoconstriction induced by pyramidal cells requires AP firing and is partially dependent on**
172 **glutamatergic transmission.**

173 In pyramidal cells, APs induce both somatic Ca²⁺ elevation (Smetters et al., 1999) and
174 glutamate release. To determine whether spiking activity is required for vasoconstriction
175 induced by 20 Hz photostimulation, we blocked APs with the voltage-activated sodium
176 channel blocker tetrodotoxin (TTX, 1 μ M, n= 6 arterioles). This treatment completely
177 abolished the vasoconstriction evoked by 20 Hz photostimulation (Fig. 3; AUC= $0.4 \pm 0.4 \times$
178 10^3 %·s, $t_{(14)} = 5.57$, p= 8.6656×10^{-6}). These data indicate that APs are mandatory for
179 neurogenic vascular response and may involve glutamate release.

180 Indeed, high levels of glutamate released from pyramidal cells may activate NPY-expressing
181 interneurons or astrocytes through activation of ionotropic or group I metabotropic glutamate
182 receptors (Girouard et al., 2010; Mulligan and MacVicar, 2004; Uhlirva et al., 2016). It may
183 also directly activate NMDA receptors on arteriolar smooth muscle cells, resulting in a large
184 intracellular Ca²⁺ increase and subsequent vasoconstriction (Zhang et al., 2024). To test the
185 hypothesis that glutamate from pyramidal cells, either directly or indirectly, results in
186 vasoconstriction, we blocked glutamatergic transmission by antagonizing AMPA/kainate,
187 NMDA and group I metabotropic receptors expressed by cortical neurons (Tasic et al., 2016;
188 Zeisel et al., 2015) and juvenile astrocytes (Sun et al., 2013). Glutamate receptor antagonists

189 reduced the magnitude of vasoconstriction ($-1.6 \pm 0.4 \times 10^3 \%$.s, $t_{(18)} = 3.28$, $p = 0.0160$) by
190 approximately half (Fig. 3). Taken together, our data suggest that photostimulation of
191 pyramidal cells elicits a frequency-dependent vasoconstriction that requires AP firing and
192 partially involves glutamatergic transmission. We therefore sought to elucidate the
193 glutamate-independent vasoactive pathway underlying this neurogenic vascular response.

194 **Pyramidal cells express the mRNAs for a cell autonomous PGE2 and PGF2 α synthesis**

195 Several arachidonic acid metabolites produced after intracellular Ca²⁺ elevation, including
196 PGF2 α , but also PGE2, exert dose-dependent vasoconstrictive effects (Dabertrand et al., 2013;
197 Rosehart et al., 2021; Zonta et al., 2003). These prostaglandins could therefore be
198 progressively released as the frequency of photostimulation and somatic Ca²⁺ increase and
199 thereby promote vasoconstriction. Layer II-III pyramidal cells have been shown to produce
200 PGE2 (Lacroix et al., 2015). To determine whether the synthesizing enzymes of PGE2 and
201 PGF2 α are present in pyramidal cells, we performed single-cell RT-PCR after patch-clamp
202 recording (Devienne et al., 2018). Sixteen layer II-III pyramidal cells were visually identified
203 based on the triangular shape of their soma and a prominent apical dendrite. Their
204 glutamatergic phenotype was confirmed both by their stereotypical regular spiking firing
205 pattern (Fig. 4a) and also by the expression of the vesicular glutamate transporter, vGlut1, and
206 neither of the two GABA synthesizing enzymes, thus excluding possible contamination by
207 GABAergic interneurons (Fig. 4b) (Karagiannis et al., 2009). The rate-limiting enzymes of
208 prostaglandin synthesis, cyclooxygenase-1 (COX-1) and -2 (COX-2), were detected in 25% ($n =$
209 4 of 16 cells) and 31% ($n = 5$ of 16 cells) of pyramidal cells, respectively, (Fig. 4b-d) but were
210 never co-expressed (Fig. 4d). Although the differential expression of COX-1 or COX-2 allowed
211 the definition of three non-overlapping molecular subpopulations of pyramidal cells, they did
212 not show distinctive electrophysiological features (supplementary Table 3). The cytosolic
213 enzyme responsible for synthesizing PGE2 (cPGES) was observed in most pyramidal cells (Fig.
214 4b-c; 88%, $n = 14$ of 16 cells). In addition, the microsomal PGES, mPGES1 and mPGES2 were
215 detected in 6% (Fig. 4c, $n = 1$ of 16 cells) and 38% (Fig. 4b,c; $n = 6$ of 16 cells) of pyramidal cells,
216 respectively, and were always co-expressed with cPGES. The PGF2 α terminal-synthesizing
217 enzyme AKR1B3 was observed in the majority of neurons (Fig. 4b-c; $n = 11$ of 16 cells, 69%).
218 Occasionally, it was co-detected with the prostamide/prostaglandin F synthase (PM-PGFS, Fig.
219 4c, $n = 5$ of 16 cells, 31%) and the PGE2 converting enzyme carbonyl reductase 1 (CBR1, Fig.

220 4c; n= 3 of 16 cells, 19%). CBR1 was consistently detected alongside at least one PGES.
221 Pyramidal cells positive for COX-1 also expressed PGES (Fig. 4d), with most of them also co-
222 expressing PGFS (n=3 out of 4). All neurons positive for COX-2 co-expressed both PGES and
223 PGFS (Fig. 4d). These molecular observations suggest that subpopulations accounting for
224 about half of layer II-III pyramidal cells express all the transcripts necessary for the synthesis
225 of PGE2 and PGF2 α .

226 **Prostaglandins underpin vasoconstriction *ex vivo* and *in vivo*.**

227 To investigate whether prostaglandins could mediate neurogenic vasoconstriction, we
228 inhibited their synthesis. In cortical slices, the non-selective COX inhibitor indomethacin (5
229 μ M, supplementary Table 4, Fig. 5a and b) completely abolished the vascular response (n= 10
230 arterioles, AUC= $0.0 \pm 0.2 \times 10^3$ % \cdot s, $t_{(18)} = 5.86$, $p = 3.4385 \times 10^{-5}$). To verify that high-frequency
231 stimulation of pyramidal cells also induces vasoconstriction *in vivo*, 10 Hz photostimulation
232 was reproduced in anesthetized Emx1-cre;Ai32 mice. Pial arterioles diameter measured by 2-
233 photon line scan imaging (Fig. 5c and d) revealed that pyramidal cells induce vasodilation (1st
234 phase) followed by sustained vasoconstriction (2nd phase, Fig. 5d and e). The constriction
235 phase was inhibited by indomethacin (i.v.), indicating the involvement of prostaglandins in the
236 vasoconstriction (AUC_{Ctrl}= -291.5 ± 92.4 % \cdot s vs. AUC_{Indo.}= 332.4 ± 184.4 % \cdot s, $U_{(5,4)} = 0$, $p = 0.0159$,
237 Fig. 5d-f), which confirms our *ex vivo* observations. To determine whether they originated
238 from COX-1 or COX-2 activity, we utilized selective inhibitors in cortical slices. The
239 vasoconstriction magnitude was reduced by the COX-1 inhibitor SC-560 (100 nM, n= 10
240 arterioles, supplementary Table 4) ($-1.4 \pm 0.7 \times 10^3$ % \cdot s, $t_{(18)} = 3.54$, $p = 9.3396 \times 10^{-3}$, Fig. 5a-b).
241 The COX-2 inhibitor NS-398 (10 μ M, n= 7 arterioles, supplementary Table 4) completely
242 abolished pyramidal cell-induced vasoconstriction in a more potent manner (Fig. 5a-b; AUC=
243 $0.1 \pm 0.3 \times 10^3$ % \cdot s, $t_{(15)} = 5.45$, $p = 1.0853 \times 10^{-5}$), mimicking the *ex vivo* effect of indomethacin.
244 These observations suggest that prostaglandins, derived mainly from COX-2 activity, and to a
245 lesser extent from COX-1 activity, mediate pyramidal cell-induced vasoconstriction.

246 **PGE2 mediates vasoconstriction by acting primarily on EP1 receptor.**

247 To determine the nature of the prostaglandins and their receptors, we selectively antagonized
248 the vasoconstrictor receptors of PGE2, EP1 or EP3, or the FP receptor of PGF2 α . The
249 magnitude of vasoconstriction was reduced by the selective EP1 receptor antagonist ONO-
250 8130 (10 nM, n= 9 arterioles, Fig. 5g-h, $0.3 \pm 0.3 \times 10^3$ % \cdot s, $t_{(17)} = 6.01$, $p = 2.8451 \times 10^{-6}$,

251 supplementary Table 4), and to a lesser extent, by the EP3 receptor antagonist L-798,106 (1
252 μM , $n = 9$ arterioles, Fig. 5 g-h, $-0.9 \pm 0.4 \times 10^3 \%$.s, $t_{(17)} = 4.30$, $p = 8.0261 \times 10^{-4}$, supplementary
253 Table 4). Impairing FP receptor signaling with AL-8810 (10 μM , $n = 9$ arterioles, Fig. 5 g-h,
254 Supplementary table 4) tended to reduce the evoked vasoconstriction, however, it did not
255 reach statistical significance (AUC= $-1.9 \pm 0.4 \times 10^3 \%$.s, $t_{(17)} = 2.82$, $p = 0.0533$). Additionally, the
256 pre-constricted state induced by this weak partial FP agonist(Sharif and Klimko, 2019)
257 (supplementary Fig. 6f) resulted in a diameter reduction of approximately 4% (diameter
258 before application $21.8 \pm 2.5 \mu\text{m}$ vs. during $20.9 \pm 2.6 \mu\text{m}$, $n = 9$ arterioles, $t_{(8)} = 2.374$, $p =$
259 0.0457 , paired t-test), which underestimated the optogenetic vascular response. Taken
260 together, these results indicate that pyramidal cell photoactivation induces vasoconstriction
261 through the release of PGE2 originating mainly from COX-2. This effect primarily acts on the
262 EP1 receptor and, to a lesser extent, on the EP3 receptor.

263 To test a direct effect of PGE2 through vascular EP1/EP3 activation, we determined whether
264 exogenous agonists of PGE2 receptors could mimic the vasoconstriction induced by pyramidal
265 cell photostimulation. Similar to increasing photostimulation frequencies, exogenous
266 application of PGE2 induced vasoconstriction in a dose-dependent manner which persisted
267 for several minutes after removal (Supplementary Fig. 7a). Likewise, 10 μM sulprostone, an
268 EP1/EP3 agonist with an EC_{50} comparable to that of PGE2 (Boie et al., 1997), mimicked the
269 vasoconstriction induced by 1-10 μM PGE2 (Supplementary Fig. 7b). Application of 10 μM
270 PGE2 in the presence of TTX did not impair the evoked vasoconstriction (Supplementary Fig.
271 7c). These observations suggest that PGE2 and its EP1 and EP3 receptors mediate a sustained
272 neurogenic vasoconstriction and that once PGE2 is released, its constrictive effect is
273 independent of AP firing.

274 **Astrocytes through 20-HETE and NPY interneurons are indirect intermediates of pyramidal** 275 **cell-induced vasoconstriction.**

276 In addition to smooth muscle cells, PGE2 released by pyramidal cells can also activate
277 astrocytes and neurons (Clasadonte et al., 2011; Di Cesare et al., 2006), which also express its
278 receptors (Tasic et al., 2016; Zeisel et al., 2015). To assess whether astrocytes could mediate
279 the PGE2-dependent vasoconstriction, we first targeted the large conductance Ca^{2+} -activated
280 (BK) channels and the 20-HETE pathways, both of which mediate astrocyte-derived
281 vasoconstriction dependent on glutamatergic transmission (Girouard et al., 2010; Mulligan

282 and MacVicar, 2004). Blockade of BK channels with paxilline (1 μ M, n= 10 arterioles,
283 Supplementary table 4) did not impair the vascular response (Fig. 6; AUC = $-3.7 \pm 0.3 \times 10^3$ %·s,
284 $t_{(18)} = 0.03$, $p = 1$). Selective inhibition of the 20-HETE synthesizing enzyme, CYP450 ω -
285 hydroxylase, with HET-0016 (100 nM, n= 10 arterioles, Supplementary table 4) reduced the
286 magnitude of the evoked vasoconstriction (Fig. 6; AUC = $-1.6 \pm 0.7 \times 10^3$ %·s, $t_{(18)} = 3.32$, $p =$
287 0.0160). These data suggest that astrocytes partially mediate the vasoconstriction induced by
288 pyramidal cells via 20-HETE but not via K^+ release. We next determined whether NPY, a potent
289 vasoconstrictor (Cauli et al., 2004), was involved in neurogenic vasoconstriction. Antagonism
290 of the NPY Y1 receptors by BIBP3226 (1 μ M, n= 10 arterioles, Supplementary table 4) abolished
291 neurogenic vasoconstriction (Fig. 6; AUC = $-0.3 \pm 0.2 \times 10^3$ %·s, $t_{(18)} = 5.28$, $p = 1.9512 \times 10^{-5}$).
292 These results suggest that neurogenic vasoconstriction induced by pyramidal cell
293 photostimulation involves NPY release and the activation of Y1 receptors (Cauli et al., 2004;
294 Karagiannis et al., 2009; Uhlirova et al., 2016) and astrocytes via 20-HETE in a glutamatergic-
295 dependent and -independent manner.

296 Discussion

297 This study establishes that pyramidal cell activity leads to arteriolar vasoconstriction, and that
298 the magnitude of the vasoconstriction depends on AP firing frequency and correlates with a
299 graded increase in pyramidal cell somatic Ca^{2+} . This vascular response partially involves
300 glutamatergic transmission through direct and indirect mechanisms on arteriolar smooth
301 muscle cells. *Ex vivo* and *in vivo* observations revealed that PGE₂, predominantly produced by
302 layer II-III COX-2 pyramidal cells, and its EP1 and EP3 receptors play a crucial role in neurogenic
303 vasoconstriction. Pharmacological evidence indicates that some interneurons, via NPY release
304 and activation of Y1 receptors, and to a lesser extent, astrocytes through 20-HETE and possibly
305 COX-1 derived PGE₂ play an intermediary role in this process (Figure 7).

306 We found that increasing the frequency of photostimulation in an *ex vivo* preparation caused
307 nearby arteriole to go from a barely discernible response to robust vasoconstriction. In
308 contrast, *in vivo* observations in anesthetized animals, with slower NVC compared to awake
309 animals (Rungta et al., 2021; Uhlirva et al., 2016), have shown that the optogenetic
310 stimulation of pyramidal cells results in a biphasic response: a fast hyperemic/vasodilatory
311 response (Kahn et al., 2013; Lacroix et al., 2015; Scott and Murphy, 2012), which can be
312 followed by a pronounced vasoconstriction (Fig. 5) (Uhlirva et al., 2016). The slow kinetics of
313 the vascular response observed *ex vivo* is comparable with previous observations in slices
314 (Cauli et al., 2004; Rancillac et al., 2006), and is likely due to the lower recording temperature
315 compared to *in vivo*, which slows the synthesis of vasoactive mediators (Rancillac et al., 2006)
316 and downstream reactions. The difficulty in observing vasodilation in cortical slices may be
317 due to relaxed arterioles which favor vasoconstriction (Blanco et al., 2008). The evidence that
318 neurogenic vasoconstriction is frequency-dependent (Fig. 1) and that pharmacologically-
319 induced vasoconstriction persists in preconstructed (Girouard et al., 2010) or pressurized
320 arterioles (Dabertrand et al., 2013), suggests that the neurogenic vasoconstriction primarily
321 depends on a high pyramidal cell firing rate rather than on vascular tone.

322 Most previous observations did not report a decreased in CBF induced by optogenetic
323 stimulation of pyramidal cells *in vivo* (Lacroix et al., 2015; Scott and Murphy, 2012). This may
324 be attributed to differences in the photostimulation paradigm and/or the specific subtype of
325 pyramidal cells that were stimulated. In our study, we used 10 seconds of photostimulation
326 both *in vivo* and *ex vivo*. Earlier studies have employed shorter photostimulation times, lasting

327 no more than 1 second (Lacroix et al., 2015; Scott and Murphy, 2012; Uhlirova et al., 2016),
328 which may have resulted in an insufficient number of elicited APs to induce robust
329 vasoconstriction. Furthermore, we observed that neurogenic vasoconstriction is highly
330 dependent on COX-2, which is primarily expressed in layer II-III pyramidal cells (Lacroix et al.,
331 2015; Tasic et al., 2016; Zeisel et al., 2015). In our study, photostimulation of almost all
332 pyramidal cells in Emx1-Cre;Ai32 mice (Gorski et al., 2002; Madisen et al., 2012) likely resulted
333 in the release of more COX-2 metabolites. Thy1-ChR2 mice used in previous studies (Scott and
334 Murphy, 2012; Uhlirova et al., 2016), on the other hand, express primarily ChR2 in layer V
335 pyramidal cells (Kahn et al., 2013) which more rarely express COX-2.

336 Our *ex vivo* and *in vivo* observations revealed that PGE2, primarily derived from COX-2, plays
337 a critical role in neurogenic vasoconstriction by activating EP1 and EP3 receptors expressed by
338 vascular smooth muscle cells (Zhang et al., 2024). Previous studies have shown that COX-2
339 pyramidal cells, when activated *in vivo* by sensory stimulation or *ex vivo*, induce a NMDA-
340 dependent increase in CBF and vasodilation through PGE2 and EP2/EP4 receptors (Lacroix et
341 al., 2015; Lecrux et al., 2011; Niwa et al., 2000). Differences in the levels and/or sites of action
342 of released PGE2 may explain the absence of secondary vasoconstriction. In Emx1-Cre;Ai32
343 mice (Gorski et al., 2002; Madisen et al., 2012), optogenetic stimulation may have activated a
344 greater number of COX-2 pyramidal cells and resulted in a higher local release of PGE2
345 compared to sensory stimulation. Furthermore, since PGE2 is barely catabolized in the
346 cerebral cortex (Alix et al., 2008), most of its removal occurs across the blood-brain barrier by
347 specific transporters. The lack of blood perfusion in brain slices may impair this clearance
348 mechanism, leading to PGE2 accumulation. It is noteworthy that the PGE2-induced
349 vasoconstriction persisted after its removal (supplementary figure 7). A high level of PGE2 may
350 have facilitated the activation of the EP1 receptor, which has a lower affinity than the EP2/EP4
351 receptors (Boie et al., 1997). Additionally, it may have promoted the rapid desensitization of
352 the dilatory EP4 receptor (Desai et al., 2000) thereby favoring vasoconstriction. Furthermore,
353 PGE2 can induce either EP1-dependent arteriolar dilation or constriction depending on
354 whether it is locally applied to capillaries or arterioles. Constriction prevails when both
355 segments are exposed (Rosehart et al., 2021). Our photostimulation focused on superficial
356 penetrating arterioles, which lack a capillary network in their close vicinity (Kasischke et al.,
357 2011). This may have facilitated the direct EP1-mediated arteriolar constriction (Dabertrand

358 et al., 2013; Rosehart et al., 2021). Overall, these observations suggest that COX-2 pyramidal
359 cells can sequentially promote both vasodilation and vasoconstriction through the release of
360 PGE₂, depending on the context.

361 Consistent with previous reports in rodents (Lacroix et al., 2015; Tasic et al., 2016; Yamagata
362 et al., 1993; Zeisel et al., 2015), the transcripts of the rate-limiting enzymes COX-1 and COX-2,
363 were detected in subpopulations of mouse layer II-III pyramidal cells, respectively. COX-1/2
364 expression was found to be systematically associated with at least one PGE₂ synthesizing
365 enzyme. The major isoforms were cPGES and mPGES₂, with the latter being less prevalent
366 (Lacroix et al., 2015; Tasic et al., 2016; Zeisel et al., 2015). The low detection rate of mPGES₁,
367 an isoform co-induced with COX-2 by various stimuli (Takemiya et al., 2007; Yamagata et al.,
368 2001), reflects its low constitutive basal expression level. The presence of PM-PGFS, CBR1 and
369 AKR1B3 in layer II-III pyramidal cells is consistent with single-cell RNAseq data (Tasic et al.,
370 2016; Zeisel et al., 2015). The expression of a PGFS was systematically observed in COX-2
371 positive pyramidal cells and in a majority of COX-1 positive neurons, similar to PGES. These
372 observations collectively indicate that subpopulations of layer II-III pyramidal cells express the
373 mRNAs required for PGE₂ and PGF₂ α synthesis derived from COX-1 or COX-2 activity. Our
374 pharmacological observations did not reveal a contribution of PGF₂ α in neurogenic
375 vasoconstriction, despite the potential ability of pyramidal cells to produce it. This is likely
376 because PGF₂ α is only detectable in pyramidal neurons under conditions where COX-2 is over-
377 expressed (Takei et al., 2012).

378 Pyramidal cells may have an indirect effect on vascular activity through the activation of
379 intermediate cell types, in addition to the direct vascular effects of PGE₂ and glutamate (Zhang
380 et al., 2024). Consistent with previous observations, we found that glutamate transmission
381 from pyramidal cells is involved to some extent (Uhlirva et al., 2016). Additionally, we found
382 that the NPY Y1 receptor plays a key role in neurogenic vasoconstriction. It is likely that
383 glutamatergic transmission contributed to NPY release, considering that NPY GABAergic
384 interneurons express a wide range of ionotropic and metabotropic glutamate receptors (Tasic
385 et al., 2016; Zeisel et al., 2015). Consistently, the Y1 receptor has been shown to be involved
386 in vasoconstriction induced by sensory and optogenetic stimulation of GABAergic
387 interneurons (Uhlirva et al., 2016). Activation of group I metabotropic receptors in
388 perivascular astrocytes has been shown to promote vasoconstriction via BK channel-

389 dependent K⁺ release (Girouard et al., 2010) or 20-HETE (Mulligan and MacVicar, 2004).
390 However, the neurogenic vasoconstriction was not affected by the blockade of BK channels,
391 which rules out this astrocytic pathway. In contrast, the inhibition of ω -hydroxylase partially
392 reduced neurogenic vasoconstriction, suggesting the involvement of 20-HETE. Additionally,
393 astrocytes may also have contributed to vasoconstriction through the release of PGE2 derived
394 from COX-1 (Attwell et al., 2016), as indicated by its mild impairment under SC-560.

395 The observation that both EP1 and Y1 antagonists abolished the vasoconstriction suggests
396 that PGE2 and NPY may act in series and/or in a more complex manner involving their
397 neuronal receptors. One possibility is that PGE2 activates NPY interneurons via the EP1
398 receptor. However, NPY interneurons barely express its transcript (Tasic et al., 2016; Zeisel et
399 al., 2015) and PGE2 constricts arterioles independently of AP firing, suggesting a direct
400 vascular effect of PGE2. Nevertheless, PGE2 may have facilitated NPY release via pre- and
401 postsynaptic EP2-signaling which have been shown to facilitate glutamate release (Sang et al.,
402 2005) and to induce neuronal firing (Clasadonte et al., 2011), respectively. On the other hand,
403 in addition to smooth muscle cells, Y1 receptors are also enriched in pyramidal (Smith et al.,
404 2019), including COX-2 positive ones (Tasic et al., 2016), and this receptor has been shown to
405 increase extracellular glutamate in the hippocampus (Meurs et al., 2012). By promoting
406 glutamate and possibly PGE2 release, neuronal activation of the Y1 receptor by NPY may also
407 have favored direct (*i.e.* PGE2) and indirect (*i.e.* 20-HETE) vasoconstrictive pathways. The
408 combined activation of vascular and neuronal Y1 receptors may explain the complete blockage
409 of optogenetically induced vasoconstriction by its antagonist BIBP3226. In *ex vivo* relaxed
410 arterioles, where vasoconstriction is favored (Blanco et al., 2008), G_q or G_i signaling of EP1 or
411 Y1 receptors, respectively, appears sufficient to induce vasoconstriction. *In vivo*, where blood
412 flow both induces myogenic tone and allows PGE2 clearance, NPY and PGE2 could also
413 synergistically promote vasoconstriction by decreasing and increasing cAMP and Ca²⁺ levels,
414 respectively, in smooth muscle cells. PGE2 and NPY may also exert temporally distinct
415 vasoconstrictor effects. Indeed, exogenous application of NPY induces a rapid and transient
416 vasoconstriction that returns to baseline levels after removal (Cauli et al., 2004), whereas
417 PGE2-induced vasoconstriction is slower and more persistent (supplementary figure 7). The
418 more transient effect of NPY likely reflects the presence of multiple NPY-degrading enzymes
419 (Wagner et al., 2015) and/or the desensitization of the Y1 receptor (Gicquiaux et al., 2003,

420 2002; Tsurumaki et al., 2002) which is not the case for PGE2(Alix et al., 2008) and its
421 vasoconstrictor receptors.

422 In awake mice, synchronous pyramidal cell activity occurs in the absence of any stimulus
423 during the so-called resting state, but it is observed at a much lower frequency than that which
424 triggers vasoconstriction and is associated with increased blood volume (Ma et al., 2016).
425 Therefore, neurogenic vasoconstriction described here is unlikely to occur under these
426 conditions. Brief sensory stimulation increases pyramidal cell activity and largely causes
427 vasodilation in both awake and anesthetized animals (Rungta et al., 2021). This hyperemic
428 response can be followed by delayed vasoconstriction (Devor et al., 2007) and involves NPY/Y1
429 receptor signaling (Uhlirova et al., 2016), similar to the mechanisms reported here. It remains
430 unclear whether PGE2 signaling is also involved in this secondary response. During prolonged
431 sensory stimulation the evoked hyperemic response appears to be more restricted to the
432 activated area at the end of the stimulation than at the beginning (Berwick et al., 2008). It is
433 possible that neurogenic vasoconstriction contributes to the later spatial confinement of the
434 vascular response. The time-locked photostimulation of virtually all pyramidal cells leading to
435 vasoconstriction would have resulted in hypersynchrony, a phenomenon that can be observed
436 during sleep/wake transitions (Asadi-Pooya and Sperling, 2019). A decrease in hemodynamics
437 has been reported during the transition from rapid eye movement sleep to wakefulness
438 (Gheres et al., 2023; Tsai et al., 2021), possibly involving neurogenic vasoconstriction.
439 Hypersynchrony is also observed in pathological conditions such as epileptic seizures (Jiruska
440 et al., 2013) and in early stages of Alzheimer's disease (Bezzina et al., 2015; Palop et al., 2007).
441 Although vasoconstriction observed in epilepsy (Farrell et al., 2016) exhibits similarities to the
442 neurogenic vasoconstriction described herein, there are notable differences between the two.
443 Like neurogenic vasoconstriction, seizure-induced hypoperfusion is dependent on COX-2
444 (Farrell et al., 2016; Tran et al., 2020) and, to some extent on PGE2 (Farrell et al., 2016), likely
445 through EP1 and/or EP3 receptors. However, epileptic seizures induce the overexpression of
446 both COX-2 and mPGES1 (Takemiya et al., 2007; Yamagata et al., 1993) as well as the ectopic
447 expression of NPY (Baraban, 2004). Similar transcriptional upregulations have also been
448 reported in Alzheimer's disease (Bezzina et al., 2015; Chaudhry et al., 2008; Palop et al., 2007;
449 Pasinetti and Aisen, 1998) Additionally, PGF2 α synthesis by COX-2 pyramidal cells is also
450 observed during seizures (Takei et al., 2012). Taken together, these observations suggest that

451 the mechanisms governing neurogenic vasoconstriction are exacerbated in pathological
452 hypersynchrony and may represent potential therapeutic targets.

453 This neurogenic vasoconstriction, observed during strong pyramidal cell activity, may seem
454 counterintuitive as it would lead to an undersupply of energy substrates despite a high energy
455 demand. However, vasoconstriction has been reported contralateral to the main activated
456 area, despite bilateral increases in neuronal activity and blood glucose uptake (Devor et al.,
457 2008), suggesting that neurogenic vasoconstriction play a physiological role. Through
458 glutamate uptake by astrocytes, neuronal activity stimulates blood glucose uptake and lactate
459 release (Pellerin and Magistretti, 1994; Voutsinos-Porche et al., 2003). In addition to its role
460 as an oxidative energy substrate for cortical neurons, lactate is also a signaling molecule that
461 enhances their spiking activity (Karagiannis et al., 2021). Therefore, uncontrolled lactate
462 supply and metabolism could potentially lead to deleterious hyperactivity (Cauli et al., 2023;
463 Sada et al., 2015). Thus, the purpose of neurogenic vasoconstriction may be to restrict energy
464 delivery to prevent an overexcitation of the cortical network.

465 Here, using multidisciplinary approaches, we describe a new mechanism of vasoconstriction
466 that depends on a high firing rate of pyramidal cells. This neurogenic vasoconstriction
467 primarily involves the release of COX-2-derived PGE2 and activation of EP1 and EP3 receptors.
468 It is mediated by direct effects on vascular smooth muscle cells but also by indirect
469 mechanisms involving NPY release from GABAergic interneurons and astrocytes by 20-HETE
470 synthesis. In contrast to previously described mechanisms of neurogenic vasoconstriction,
471 that have been mostly associated with GABAergic interneurons and neuronal inhibition (Cauli
472 et al., 2004; Devor et al., 2007; Krawchuk et al., 2020; Lee et al., 2020; Uhlirova et al., 2016),
473 our data suggest the involvement of glutamatergic excitatory neurons and increased neuronal
474 activity. This finding will help to update the interpretation of the functional brain imaging
475 signals used to map network activity in health and disease (Iadecola, 2017; Zhang and Raichle,
476 2010). This excitatory form of neurogenic vasoconstriction may also help to understand the
477 etiopathogenesis of epilepsy (Farrell et al., 2016; Tran et al., 2020) and Alzheimer's disease
478 (Palop and Mucke, 2010) in which increased cortical network activity and hypoperfusion often
479 overlap.

480 **Materials and methods**

481 **Animals**

482 Homozygous Emx1-Cre mice [Jackson Laboratory, stock #005628, B6.129S2-Emx1^{tm1(cre)Krl}/J
483 (Gorski et al., 2002)] were crossed with homozygous Ai32 mice [Jackson Laboratory, stock
484 #012569, B6;129S-Gt(ROSA)26Sor^{tm32(CAG-COP4*H134R/EYFP)Hze}/J (Madisen et al., 2012)] to obtain
485 heterozygous Emx1^{cre/WT};Ai32^{ChR2/WT} mice for optogenetic stimulations. C57BL/6RJ mice were
486 used for PGE2 and sulprostone exogenous applications, control optogenetic experiments and
487 single-cell RT-PCR. 16-21 postnatal day-old females and males were used for all *ex vivo*
488 experiments. Female Emx1^{cre/WT};Ai32^{ChR2/WT} mice, 3 to 5-month-old, were used for *in vivo*
489 experiments.

490 All experimental procedures using animals were carried out in strict accordance with French
491 regulations (Code Rural R214/87 to R214/130) and conformed to the ethical guidelines of the
492 European Communities Council Directive of September 22, 2010 (2010/63/UE). Mice were fed
493 *ad libitum* and housed in a 12-hour light/dark cycle. *In vivo* experiments were done in
494 accordance with the Institut national de la santé et de la recherche médicale (Inserm) animal
495 care and approved by the ethical committee Charles Darwin (Comité national de réflexion
496 éthique sur l'expérimentation animale – n°5) (protocol number #27135 2020091012114621).

497 **Ex vivo slice preparation**

498 Mice were deeply anesthetized by isoflurane (IsoVet, Piramal Healthcare UK or IsoFlo,
499 Axience) evaporation in an induction box then euthanized by decapitation. The brain was
500 quickly removed and placed in cold (~4°C), oxygenated artificial cerebrospinal fluid (aCSF)
501 containing (in mM): 125 NaCl, 2.5 KCl, 1.25 NaH₂PO₄, 2 CaCl₂, 1 MgCl₂, 26 NaHCO₃, 10
502 glucose, 15 sucrose and 1 kynurenic acid (Sigma-Aldrich). 300 µm-thick coronal slices
503 containing the barrel cortex were cut with a vibratome (VT1000s; Leica) and were allowed to
504 recover at room temperature for at least 45 min with oxygenated aCSF (95% O₂/5% CO₂)
505 (Devienne et al., 2018). The slices were then transferred to a submerged recording chamber
506 and perfused continuously at room temperature (20-25 °C) at a rate of 2 ml/min with
507 oxygenated aCSF lacking kynurenic acid.

508 **Whole-cell recordings**

509 Patch pipettes (5.5 ± 0.2 M Ω) pulled from borosilicate glass were filled with 8 μ l of RNase free
510 internal solution containing (in mM): 144 K-gluconate, 3 MgCl₂, 0.5 EGTA, 10 HEPES, pH 7.2
511 (285/295 mOsm). For electrophysiological recordings combined with calcium imaging, EGTA
512 was replaced by 200 μ M Rhod-2 (20777, Cayman chemicals). Whole-cell recordings were
513 performed using a patch-clamp amplifier (Axopatch 200B, MDS). Data were filtered at 5-10
514 kHz and digitized at 50 kHz using an acquisition board (Digidata 1440, MDS) attached to a
515 personal computer running pCLAMP 10.2 software package (MDS). Electrophysiological
516 properties were determined in current-clamp mode (Karagiannis et al., 2009). Membrane
517 potential values were corrected for theoretical liquid junction potential (-15.6 mV). Resting
518 membrane potential of neurons was measured immediately after passing in whole-cell
519 configuration. Only neurons with a resting membrane potential more hyperpolarized than -60
520 mV were analyzed further.

521 **Optogenetic stimulation**

522 Optogenetic stimulation was achieved through the objective using a 470 nm light emitting
523 device (LED, CoolLED, Precise Excite) attached to the epifluorescence port of a BX51WI
524 microscope (Olympus) and a set of multiband filters consisting of an excitation filter (HC
525 392/474/554/635, Semrock), a dichroic mirror (BS 409/493/573/652, Semrock), and an
526 emission filter (HC 432/515/595/730, Semrock). Photostimulation consisted of a 10-s train of
527 5 ms light pulses at an intensity of 38 mW/mm² and delivered at five different frequencies (1,
528 2, 5, 10 and 20 Hz).

529 **Infrared imaging**

530 Blood vessels and cells were observed in slices under infrared illumination with Dodt gradient
531 contrast optics (IR-DGC, Luigs and Neumann) using a double-port upright microscope
532 (BX51WI, Olympus) and a collimated light emitting device (LED; 780 nm; ThorLabs) as the
533 transmitted light source, a 40X (LUMPlanF/IR, 40X/0.80 W, Olympus) or a 60X (LUMPlan FL/IR
534 60X/0.90 W, Olympus) objective and a digital camera (OrcaFlash 4.0, Hamamatsu) attached to
535 the front port of the microscope. Penetrating arterioles in layer I were selected by IR-DGC
536 videomicroscopy based on their well-defined luminal diameter (10-40 μ m), their length
537 remaining in the focal plane for at least 50 μ m (Lacroix et al., 2015), and the thickness of their
538 wall (4.1 ± 0.1 μ m, n = 176 blood vessels). A resting period of at least 30 min (Zonta et al., 2003)

539 was observed after slice transfer. After light-induced responses, arteriolar contractility was
540 tested by the application of aCSF containing the thromboxane A2 agonist, U46619 (100
541 nM)(Cauli et al., 2004) or K⁺ enriched solution (composition in mM: 77.5 NaCl, 50 KCl, 1.25
542 NaH₂PO₄, 2 CaCl₂, 1 MgCl₂, 26 NaHCO₃, 10 glucose, 15 sucrose). Vessels that did not constrict
543 with these applications were discarded. Only one arteriole was monitored per slice receiving
544 a single optogenetic or pharmacological stimulation. IR-DGC images were acquired at 0.1 Hz
545 for pharmacological applications and at 1 Hz for optogenetic experiments using Imaging
546 Workbench 6.1 software (Indec Biosystems). The focal plane was continuously maintained on-
547 line using IR-DGC images of cells as anatomical landmarks(Lacroix et al., 2015).

548 **Calcium imaging**

549 Visually and electrophysiologically identified layer II-III pyramidal cells were filled with the
550 calcium-sensitive dye Rhod-2 (200 μM, Cayman chemicals, 20777) using patch pipettes.
551 Optical recordings were made at least 15 min after passing in whole-cell configuration to allow
552 for somatic diffusion of the dye. Rhod-2 was excited with a 585 nm LED (Cool LED, Precise
553 Excite) at an intensity of 0.56 mW/mm² and the filter set used for optogenetic stimulation
554 using the Imaging Workbench 6.1 software (Indec Biosystems). IR-DGC and fluorescence
555 images were acquired by alternating epifluorescence and transmitted light sources. IR-DGC
556 and fluorescence were respectively sampled at 5 Hz and 1 Hz during baseline and optogenetic
557 stimulation, respectively, and at 1 Hz and 0.2 Hz after photostimulation. During
558 photostimulation, bleed-through occurred in the Rhod-2 channel due to the fluorescence of
559 the EYFP-ChR2 transgene (Madisen et al., 2012). Therefore, the Ca²⁺ response could not be
560 reliably analyzed during this period. To compensate for potential x-y drifts, all images were
561 registered off-line using the “StackReg” plug-in (Thévenaz et al., 1998) of the ImageJ 1.53
562 software. To define somatic regions of interest (ROIs), the soma was manually delineated from
563 IR-DGC images. Fluorescence intensity changes ($\Delta F/F_0$) were expressed as the ratio $(F-F_0)/F_0$
564 where F is the mean fluorescence intensity in the ROI at a given time point, and F₀ is the mean
565 fluorescence intensity in the same ROI during the 30-s control baseline.

566 **Drugs**

567 All pharmacological compounds were bath applied after a 5-min baseline, and vascular
568 dynamics were recorded during bath application. The following drugs were dissolved in water:
569 D-(-)-2-amino-5-phosphonopentanoic acid (D-AP5, 50 μM, Hellobio, HB0225), 6,7-

570 dinitroquinoxaline-2,3-dione (DNQX, 10 μ M, Hellobio, HB0262), LY367385 (100 μ M, Hellobio,
571 HB0398) and BIBP3226 (1 μ M, Tocris, 2707). Tetrodotoxin (TTX, 1 μ M, L8503, Latoxan) was
572 dissolved in 90 % acetic acid. PGE2 (HB3460, Hellobio), sulprostone (10 μ M, Cayman chemical,
573 14765), 2-methyl-6-(phenylethynyl)pyridine (MPEP, 50 μ M, Hellobio, HB0426) and 9,11-
574 dideoxy-9 α ,11 α -methanoepoxy prostaglandin F2 α (U-46619, 100 nM, Enzo, BML-PG023)
575 were dissolved in ethanol. Indomethacin (5 μ M, Sigma-Aldrich, I7378), SC-560 (100 nM, Sigma-
576 Aldrich, S2064-5MG), NS-398 (10 μ M, Enzo, BML-EI261), ONO-8130 (10 nM, Tocris, 5406), L-
577 798,106 (1 μ M, Cayman chemical, 11129), AL8810 (10 μ M, Cayman chemical, 16735), paxilline
578 (10 μ M, Tocris, 2006) and HET0016 (100 μ M, Merck, SML2416-5MG) in DMSO. Acetic acid,
579 ethanol and DMSO doses were always used below 0.1%. Synthesis inhibitors and BIBP3226
580 were applied at least 30 minutes before optogenetic stimulation. TTX was applied at least 15
581 minutes before, while glutamate receptor antagonists and paxilline were applied at least 10
582 and 5 minutes before, respectively.

583 **Vascular reactivity analysis**

584 To compensate for potential x-y drifts, all images were realigned off-line using the “StackReg”
585 plug-in (Thévenaz et al., 1998) of the ImageJ 1.53 software. Luminal diameter was measured
586 in layer I on registered images using custom analysis software developed in MATLAB
587 (MathWorks) (Lacroix et al., 2015). To avoid potential drawbacks due to vessel instability, only
588 arterioles with a stable diameter were analyzed further. Arterioles were considered stable if
589 the relative standard deviation of their diameter during the baseline period was less than 5%
590 (Lacroix et al., 2015). Comparison of the mean arteriolar diameter during the 5-minute
591 baseline and the 5-minute final pharmacological treatments revealed that all drugs, except
592 AL8810, had no effect on resting diameter (Supplementary Fig. 4, 6 and 8).

593 Diameter changes ($\Delta D/D_0$) were expressed as $(D_t - D_0)/D_0$ where D_t is the diameter at the time
594 t and D_0 is the mean diameter during the baseline period. To eliminate sharp artifacts due to
595 transient loss of focus, diameter change traces were smoothed using a sliding three-point
596 median filter. The overall vascular response over time was captured by the area under the
597 curve of diameter changes after photostimulation. To determine the onset of
598 vasoconstriction, a Z-score was calculated from the diameter change traces using the formula:
599 $Z = (x - \mu) / \sigma$, where both the mean μ and the standard deviation σ were calculated from the
600 values before photostimulation. Onset of vasoconstriction was defined as the time after the

601 start of photostimulation at which the Z-score exceeded or fell below -a value of -1.96 (95%
602 criteria) for 10 seconds. If a vessel showed no vasoconstriction, the onset was arbitrarily set
603 at 1800 seconds. Graphs were generated using R software version 4.3.0 (Team et al., 2023)
604 and Matplotlib package (Caswell et al., 2023).

605 **Intrinsic optical signals analysis**

606 Variations in IR light transmittance (ΔT) (Zhou et al., 2010) were determined using ImageJ 1.53
607 software according to: $\Delta T = (T_t - T_0) / T_0$ where T_t is the light transmittance at a time t and T_0 is
608 the average light transmittance during the baseline period of a squared region of interest of
609 $100 \mu\text{m} \times 100 \mu\text{m}$ manually delineated in layer I. The rate of ΔT change was determined as the
610 first derivative of ΔT ($d\Delta T/dt$, where ΔT is the change in light transmittance and t is time).
611 Slices that showed a maximum rate of increase of $d\Delta T/dt$ greater than 2%/s, indicating the
612 occurrence of spreading depression (Zhou et al., 2010), were excluded.

613 **Surgery**

614 Chronic cranial windows were implanted one week after the head bar surgery as previously
615 described (Tournissac et al., 2022). We used a $100 \mu\text{m}$ thick glass coverslip over the barrel
616 cortex ($\sim 3\text{mm}^2$). Before two-photon experiments, a recovery period of 7-10 days minimum
617 was maintained.

618 **Two-photon imaging and photostimulation**

619 For two-photon excitation, we used a femtosecond laser (Mai Tai eHP; SpectraPhysics) with a
620 dispersion compensation module (Deepsee; SpectraPhysics) emitting 70-fs pulses at 80 MHz.
621 The laser power was attenuated by an acousto-optical modulator (AA Optoelectronic, MT110-
622 B50-A1.5-IR-Hk). Scanning was performed with Galvanometric scanner (GS) mirrors
623 (8315KM60B; Cambridge Technology). Fluorescein was excited at 920 nm and the emitted
624 light was collected with a LUMFLN60XW (Olympus, 1.1 NA) water immersion objective.
625 Collected photons were sorted using a dichroic mirror centered at 570 nm, a FF01-525/25 nm
626 filter (Semrock) and a GaAsP (Hamamatsu) photomultiplier tube. Customized LabView
627 software was used to control the system. Line scans were drawn across pial vessels to measure
628 the change in arterioles diameter, which are not compromised by the fluorescence from the
629 ChR2-EYFP transgene in the parenchyma (Madisen et al., 2012), are less affected by potential
630 movement in the x-y plan than in penetrating arterioles, and whose dilation dynamics are
631 similar in the somatosensory cortex (Rungta et al., 2021).

632 Mice were anesthetized with a mixture of ketamine and medetomidine (100 and 0.5 mg/kg,
633 respectively, intraperitoneal (i.p.)) during imaging sessions. Body temperature was
634 maintained at 36.5°C using a retro-controlled heating pad. Fluorescein dextran (70 kDa) was
635 injected i.v. through a retro-orbital injection to label brain vessels. Mice received continuous
636 air through a nose cone supplemented with oxygen to reach a final concentration of 30% O₂.
637 Photostimulation was delivered with a 473 nm laser (Coblot MLD, Sweden) through an optic
638 fiber placed above the glass coverslip and directed at the pial artery of interest. Each
639 photostimulation consisted of a 10-s train of 5 ms light pulses at an intensity of 1 mW delivered
640 at 10 Hz, with a 5-minute interstimulus interval to allow full recovery to baseline.
641 Indomethacin (10mg/kg, #15425529, Thermo Fisher Scientific) was administered i.v. through
642 a retroorbital injection.

643 **Imaging analysis**

644 Pial arteriole diameter change was determined with line-scan acquisitions and a home-made
645 Matlab script as previously described (Rungta et al., 2018). Trials from the same vessel were
646 averaged (with a 0.1 s interpolation) for analysis. Area under the curve and statistics were
647 performed using GraphPad Prim (version 6).

648 **Cytoplasm harvesting and single-cell RT-PCR**

649 At the end of the whole-cell recording, which lasted less than 15 min, the cytoplasmic content
650 was collected in the recording pipette by applying a gentle negative pressure. The pipette's
651 content was expelled into a test tube and RT was performed in a final volume of 10 µl as
652 described previously (Devienne et al., 2018). The scRT-PCR protocol was designed to probe
653 simultaneously the expression of prostaglandins synthesizing enzymes and neuronal markers
654 (Lacroix et al., 2015). Prostaglandins synthesizing enzymes included COX-1 and COX-2, the
655 terminal PGE₂ synthases (PGES): mPGES1, mPGES2 and cPGES, the terminal PGF₂α synthases
656 (PGFS): PM-PGFS (Prxl2b) and AKR1B3 and the carbonyl reductase CBR1. Neuronal markers
657 included the vesicular glutamate transporter, vGluT1, and the two isoforms of glutamic acid
658 decarboxylase, GAD65 and GAD67. Two-step amplification was performed essentially as
659 described (Devienne et al., 2018). First, cDNAs present in the 10 µl reverse transcription
660 reaction were simultaneously amplified with all external primer pairs listed in Supplementary
661 table 2. Taq polymerase (2.5 U; Qiagen) and external primers mix (20 pmol each) were added
662 to the manufacturer's buffer (final volume, 100 µl), and 20 cycles (95°C, 30 s; 60°C, 30 s; and
663 72°C, 35 s) of PCR were performed. Second rounds of PCR were performed using 1 µl of the

664 first PCR product as a template. In this second round, each cDNA was amplified individually
665 using its specific nested primer pair (Supplementary table 2) by performing 35 PCR cycles (as
666 described above). 10 µl of each individual PCR product were run on a 2% agarose gel stained
667 with ethidium bromide using ΦX174 digested by *HaeIII* as a molecular weight marker. The
668 efficiency of the protocol was validated using 500 pg of total forebrain RNAs (Supplementary
669 Fig. 5).

670 **Statistical analyses**

671 Statistical analyses were performed using GraphPad Prism version 7.00 for Windows
672 (GraphPad Software, La Jolla California USA, www.graphpad.com) and R software version
673 4.3.0 (Team et al., 2023). Normality of distribution was assessed using the Shapiro-Wilk tests.
674 Equality of variance was assessed using Brown-Forsythe tests for comparisons between
675 groups and using F-tests for comparisons with a control group. Parametric tests were only
676 used if these criteria were met. Statistical significance of morphological and physiological
677 properties of penetrating arterioles was determined using one-way ANOVA for comparison
678 between groups. Statistical significance of calcium was determined using two-tailed unpaired
679 t-tests and Statistical significance of vascular responses were appreciated using Tukey posthoc
680 tests for the different frequencies conditions and using Dunnett's posthoc tests for the
681 different pharmacological conditions compared to the 20 Hz condition without
682 pharmacological compound. False discovery rate correction was used for multiple
683 comparisons. Statistical significance of vascular diameter for drug applications was
684 determined using two-tailed paired t-tests. Statistical significance on all figures uses the
685 following convention: * $p < 0.05$, ** $p < 0.01$ and *** $p < 0.001$.

686 **Data availability statement**

687 The data that support the results of this study are available from the corresponding author
688 upon reasonable request.

689 **Acknowledgements**

690 The authors thank Dr Rebecca Piskorowski for constructive criticism of the manuscript. We
691 acknowledge the invaluable support of the animal facilities of IBPS (RongIBPS) and Institut de
692 la vision for their expert care and maintenance of the animals used in this study. Financial
693 support was provided by grants from the Agence Nationale pour la Recherche (ANR-17-CE37-

694 0010-03, B.C.; CE37_2020_TF-fUS-CADASIL, S.C.; ANR-20-CE14-0025, D.L.; ANR-23-CE14-
695 0038-01, B.C.), the Fondation Alzheimer France (M21JRCN009, S.C.) and the i-Bio initiative of
696 Sorbonne University (B.C.). B.L.G. and E.B. were supported by fellowships from Fondation pour
697 la Recherche sur Alzheimer and M.T. by a fellowship from the Fondation pour la Recherche
698 Médicale (SPF201909009103).

699 **Author contributions**

700 B.L.G., M.T., and E.B. designed experiments, acquired, and analyzed the data, and edited the
701 manuscript. S.P. acquired the data. B.L.G. and B.C. drafted the manuscript. I.D. edited the
702 manuscript. H.S. analyzed the data. D.L. designed experiments and edited the manuscript. S.C.
703 and B.C. designed experiments and edited the manuscript.

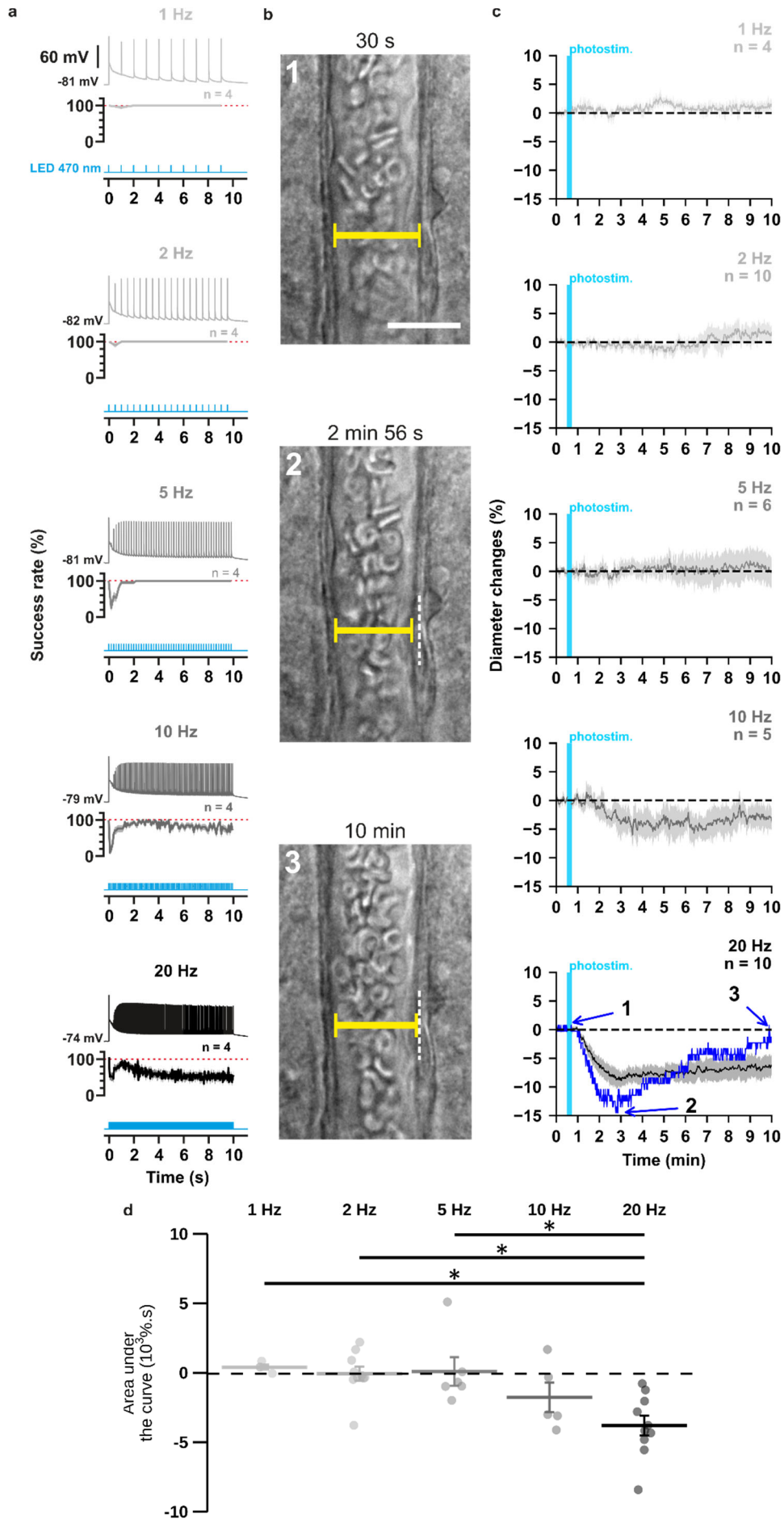


Figure 1: The occurrence and strength of vasoconstriction depends on the photostimulation frequency of pyramidal cells. **(a)** Representative examples of the voltage responses of a layer II-III pyramidal cell (upper traces light grey to black traces) induced by photostimulations (470 nm, 10 s train, 5 ms pulses) delivered at 1, 2, 5, 10 and 20 Hz (cyan lower traces) and mean spike success rate (middle trace, n= 4 cells from 3 mice). The SEMs envelope the mean traces. The red dashed lines represent a spike success rate of 100%. **(b)** Representative example showing IR-DGC pictures of a layer I penetrating arteriole (1) before a 20 Hz photostimulation, (2) at the maximal diameter decrease, and (3) after 10 minutes of recording. Pial surface is upward. Yellow calipers represent the measured diameters. White dashed lines indicate the initial position of the vessel wall. Scale bar: 25 μm . **(c)** Kinetics of arteriolar diameter changes induced by photostimulation (vertical cyan bars) at 1 Hz (n= 4 arterioles from 3 mice), 2 Hz (n= 10 arterioles from 8 mice), 5 Hz (n= 6 arterioles from 6 mice), 10 Hz (n= 5 arterioles from 5 mice) and 20 Hz (n= 10 arteriole from 9 mice). The SEMs envelope the mean traces. The blue trace represents the kinetics of the diameter changes of the arteriole shown in (b). **(d)** Effects of the different photostimulation frequencies on AUC of vascular responses during 10 min of recording. Data are presented as the individual values and mean \pm SEM. * statistically different from 20 Hz stimulation with $p < 0.05$.

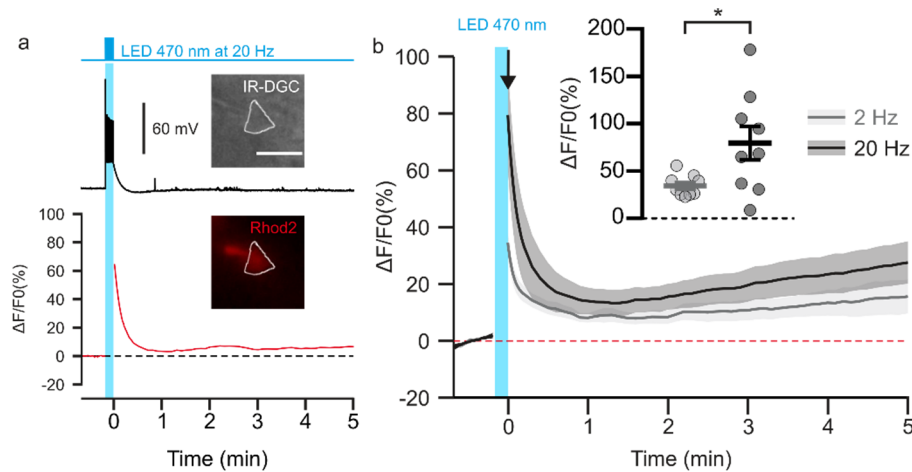


Figure 2: Photostimulation of pyramidal cells elicits a time-locked firing and a frequency-dependent calcium increase. (a). Voltage response (top trace) and kinetics of relative fluorescence changes (red bottom trace) induced by photostimulation at 20 Hz. Insets, IR-DGC (top), Rhod2 fluorescence (bottom) pictures of an imaged layer II/III pyramidal cell. The somatic region of interest is outlined in white. Pia surface is upward. Scale bar: 20 μm . **(b)** Mean relative variations of Ca^{2+} fluorescence in response to photostimulation at 2 Hz (grey) and 20 Hz (black). Dashed line represents the baseline. The vertical cyan bar indicates the duration of photostimulation. SEMs envelope the mean traces. Inset, Maximum increase in relative fluorescence changes induced immediately after photostimulation, indicated by the black arrow. The data are shown as the individual values and mean \pm SEM. * statistically different with $p < 0.05$.

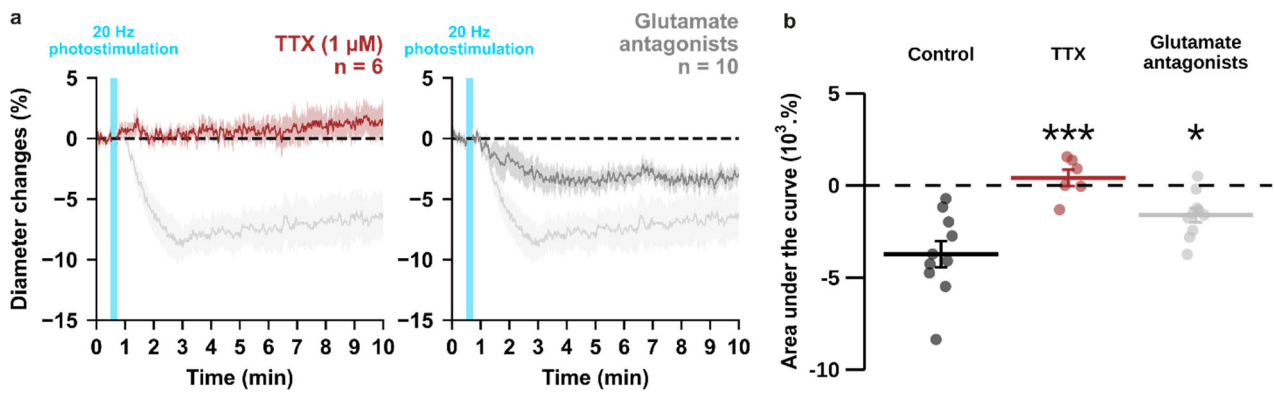


Figure 3: Optogenetically-induced vasoconstriction requires AP firing and partially glutamatergic transmission. Effect of TTX (1 μM, brown, n= 6 arterioles from 5 mice) and cocktail antagonists of AMPA/kainate (DNQX, 10 μM), NMDA (D-AP5, 50 μM), mGluR1 (LY367385, 100 μM) and mGluR5 (MPEP, 50 μM) receptors (gray, n= 10 arterioles from 6 mice) on **(a)** kinetics and **(b)** magnitude of arteriolar vasoconstriction induced by 20 Hz photostimulation (cyan bar). The SEMs envelope the mean traces. Dashed lines represent the initial diameter. The shaded traces correspond to the kinetics of arteriolar vasoconstriction in control condition (Fig. 1c – 20 Hz). Data are presented as the individual values and mean ± SEM. * and *** statistically different from control condition (Fig. 1c – 20 Hz) with $p < 0.05$ and $p < 0.001$, respectively.

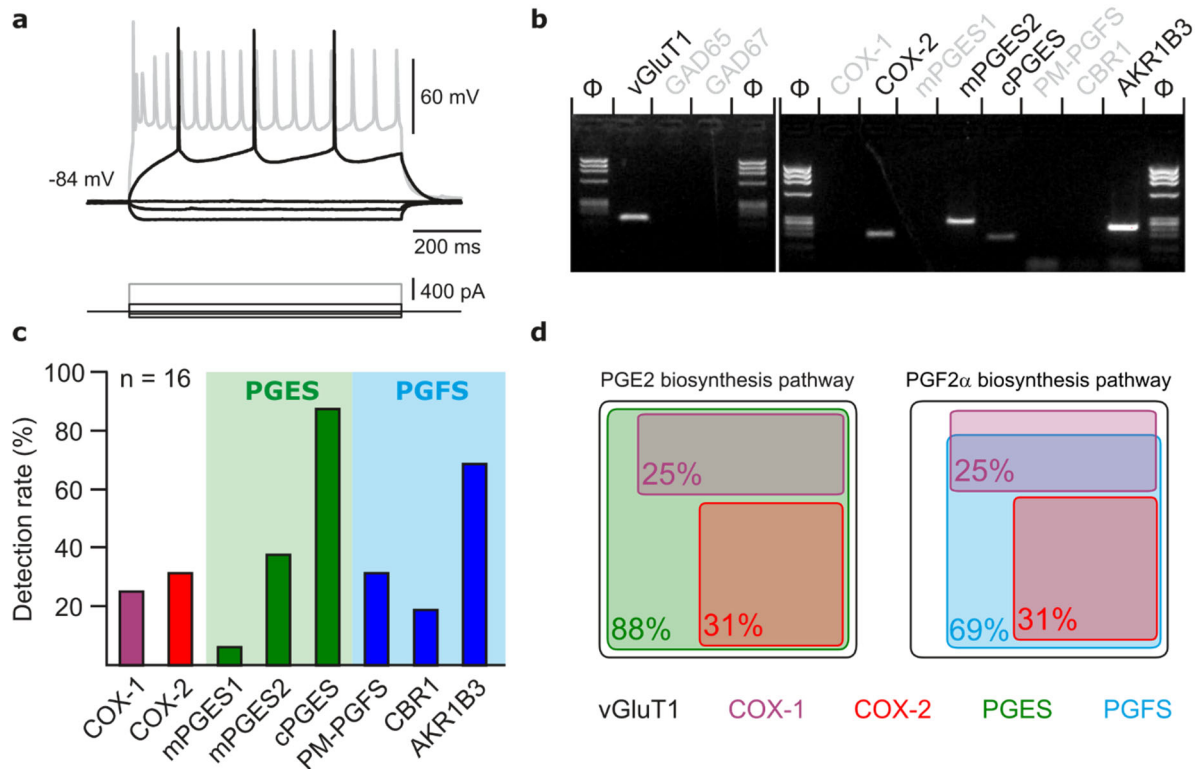


Figure 4: Layer II-III pyramidal cells express PGE2 and PGF2 α synthesizing enzymes. (a) Voltage responses of a layer II-III pyramidal cell induced by injection of current (bottom traces). In response to a just-above-threshold current pulse, the neuron fired long-lasting action potentials with little frequency adaptation (middle black trace). Near saturation, it exhibits the pronounced spike amplitude accommodation and marked frequency adaptation characteristic of regular spiking cells (upper grey trace). **(b)** Agarose gel analysis of the scRT-PCR products of the pyramidal cell shown in (a) revealing expression of vGluT1, COX-2, mPGES2, cPGES, PM-PGFS and CBR1. Φ x174 digested by *HaeIII* (Φ) was used as molecular weight marker **(c)** Histogram summarizing the single-cell detection rate of PGE2 and PGf2 α synthesizing enzymes in layer II-III pyramidal cells (n= 16 cells from 6 mice). PGES (green zone) corresponds to mPGES1, mPGES2 and/or cPGES and PGFS (blue zone) to PM-PGFS, CBR1 and/or AKR1B3. **(d)** Co-expression of PGE2 and PGf2 α synthesizing enzymes in pyramidal cells. The box size is proportional to the detection rate. Note the absence of co-expression between COX-1 (purple) and COX-2 (red). Co-expression of a PGES (left, green) and a PGFS (right, blue) with COX-1 (up) and COX-2 (bottom).

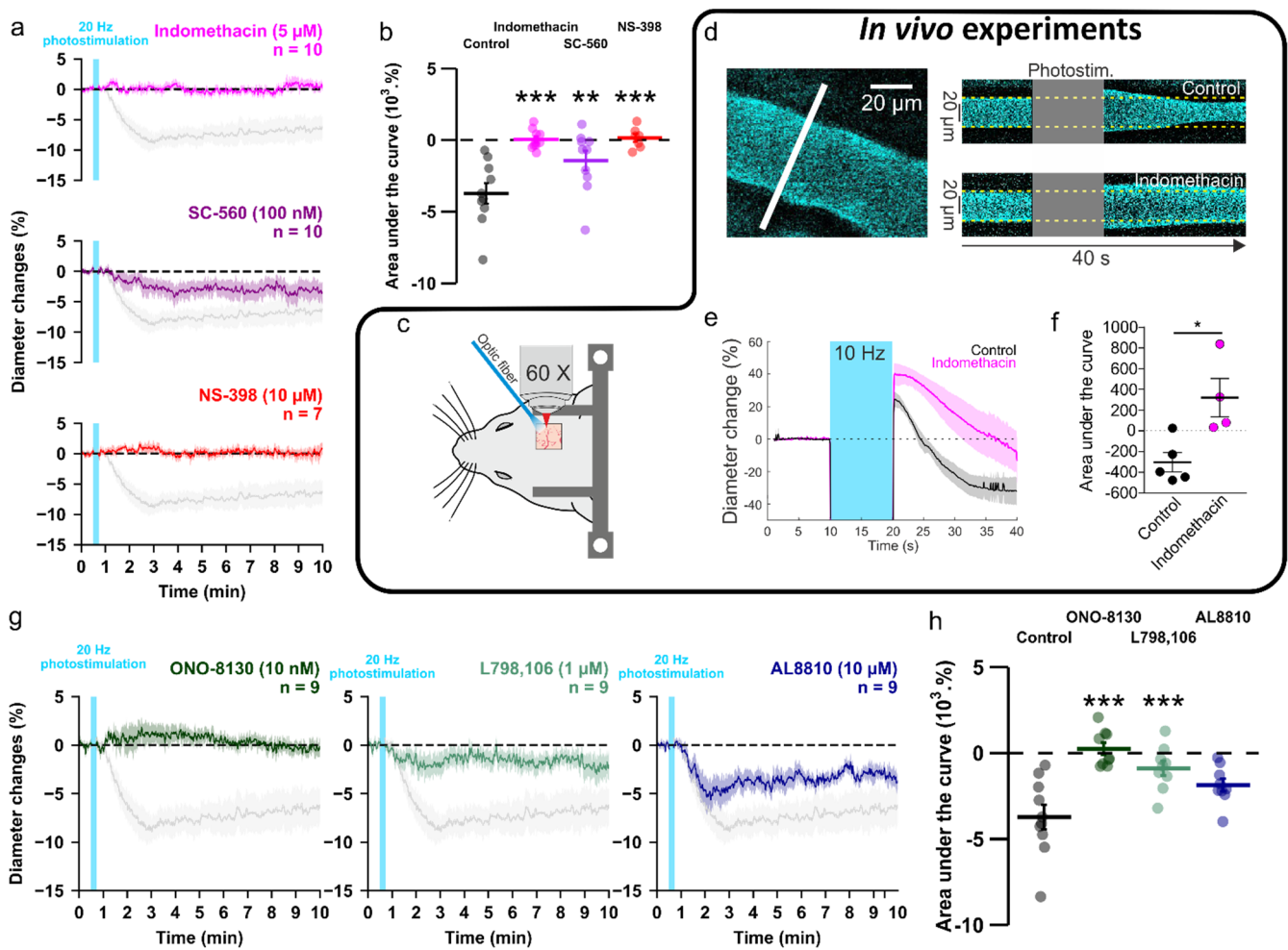


Figure 5: PGE2 mostly derived from COX-2 activity and its EP1 and EP3 receptors mediates vasoconstriction induced by optogenetically activated pyramidal cells. (a, b) *Ex vivo* effects of the COX1/2 inhibitor indomethacin (magenta, n= 10 arterioles from 9 mice), the COX-1 inhibitor SC-560 (purple, n= 10 arterioles from 7 mice), and the COX-2 inhibitor NS-398 (red, n= 7 arterioles from 6 mice) on kinetics (a) and AUC (b) of arteriolar vasoconstriction induced by 20 Hz photostimulation (vertical cyan bar). *In vivo* experiments are highlighted by a black frame. (c) Optogenetic stimulation was achieved *in vivo* with an optic fiber through a chronic cranial window over the barrel cortex. (d) Left, diameter of pial arterioles labeled with fluorescein dextran (i.v) was measured with line-scan crossing the vessel (white line). Right, Representative examples of vascular response upon photostimulation (10 Hz, 10 s) under control (top) and indomethacin condition (bottom). (e) Diameter changes upon photostimulation under control (black; n = 5 arterioles, 4 mice) or indomethacin (magenta; n = 4 arterioles, 4 mice) conditions. (f) Area under the curve of the diameter change in control (black) or indomethacin (magenta) conditions calculated between 20 and 40 s (unpaired, two-tailed Mann Whitney test, * p<0.05). (g, h) Effects of the EP1, EP3 and FP antagonists, ONO-8130 (10 nM, dark green, n= 9 arterioles from 7 mice), L798,106 (1 μM , light green, n= 9 arterioles from 5 mice) and AL8810 (10 μM , dark blue, n= 9 arterioles from 7 mice), respectively, on kinetics (g) and AUC (h) of arteriolar vasoconstriction induced by 20 Hz photostimulation. The data are shown as the individual values and mean \pm SEM. Dashed line represents the baseline. The SEMs envelope the mean traces. The data are shown as the individual values and mean \pm SEM. The shaded traces correspond to the control condition (Fig. 1c – 20 Hz). *, ** and *** statistically different from 20 Hz control condition with p< 0.05, 0.01 and 0.001, respectively.

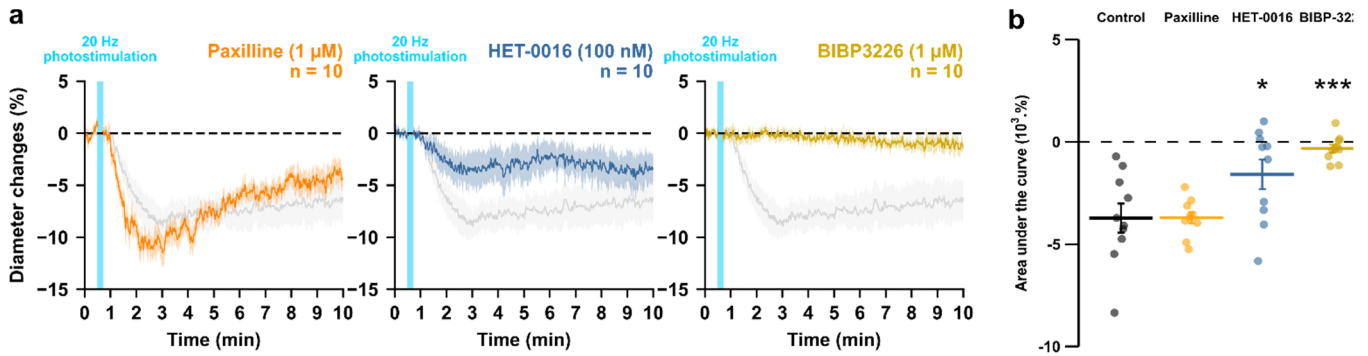


Figure 6: NPY Y1 receptors activation and 20-HETE synthesis mediates the vasoconstriction induced by pyramidal neurons. Effects of paxilline (1 μ M, orange, n = 10 arterioles from 6 mice), HET-0016 (100 nM, blue-grey, n = 10 arterioles from 7 mice) and BIBP3226 (1 μ M, yellow, n = 10 arterioles from 6 mice) on **(a)** kinetics and **(b)** AUC of arteriolar vasoconstriction induced by 20 Hz photostimulation (vertical blue bar). Dashed line represents the baseline. The SEMs envelope the mean traces. The shaded traces correspond to the control condition (Fig. 1c – 20 Hz). The data are shown as the individual values and mean \pm SEM. * and *** statistically different from 20 Hz control condition with $p < 0.05$ and 0.001 .

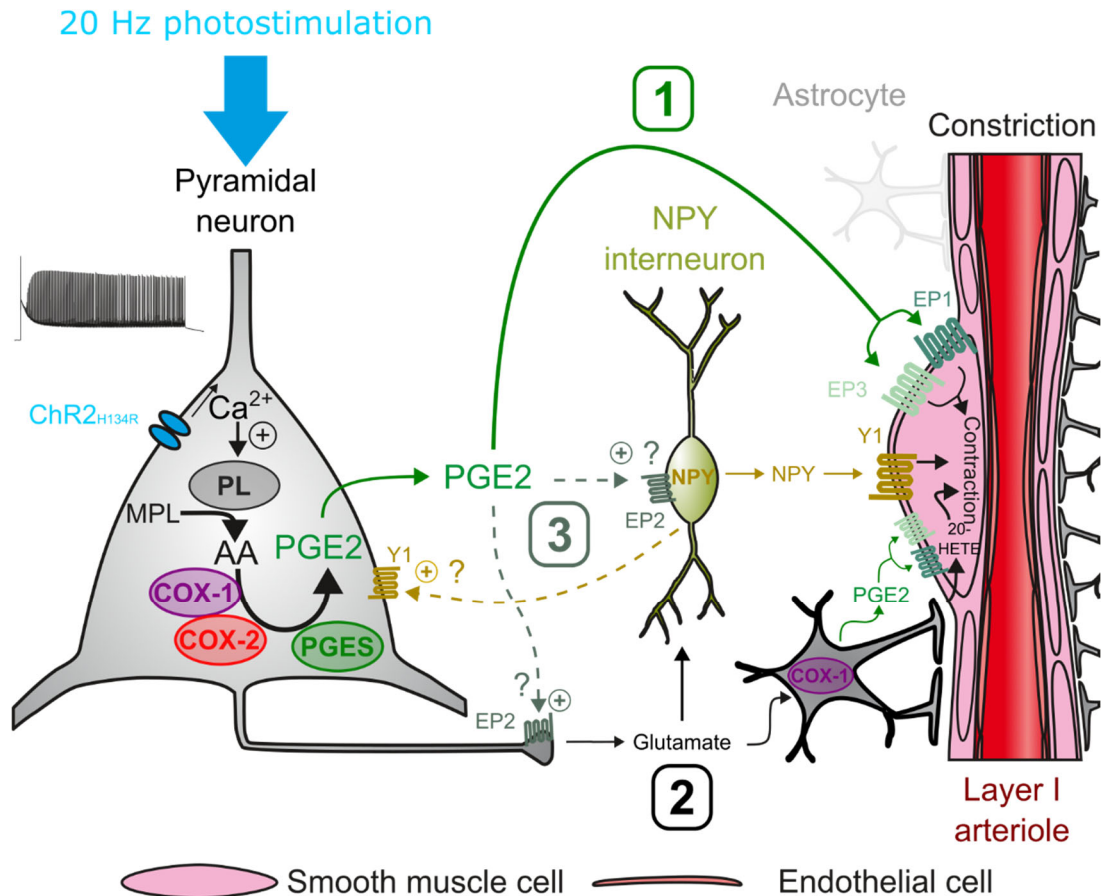


Figure 7: Possible pathways of vasoconstriction induced by pyramidal neurons. 20 Hz photostimulation induces activation of pyramidal neurons expressing channelrhodopsin-2 (ChR2_{H134R}) and increases intracellular calcium (Ca²⁺). Arachidonic acid (AA) is released from membrane phospholipids (MPL) by phospholipases (PL) activated by intracellular Ca²⁺ and is metabolized by type-1 and type-2 cyclooxygenases (COX-1 and COX-2) and prostaglandin E2 synthases (PGES) to produce prostaglandin E2 (PGE2). Three non-exclusive pathways can be proposed for arteriolar vasoconstriction in layer I: 1) PGE2 released into the extracellular space may act directly on arteriolar EP1 and EP3 receptors to induce smooth muscle cell constriction. 2) Glutamate released from pyramidal cells may activate neuropeptide Y (NPY) interneurons and NPY is released to act on vascular and neuronal Y1 receptors to constrict smooth muscle cells and promote glutamate release, respectively. Glutamate can also activate astrocytes to induce constriction through the 20-HETE and the COX-1/PGE2 pathways. 3) PGE2 may act on pre- and postsynaptic EP2 receptors to facilitate glutamate release and NPY interneuron activation, respectively.

References

- 704 Alix E, Schmitt C, Strazielle N, Ghersi-Egea JF. 2008. Prostaglandin E2 metabolism in rat brain:
705 Role of the blood-brain interfaces. *Cerebrospinal Fluid Res* **5**. doi:10.1186/1743-8454-5-5
- 706 Asadi-Pooya AA, Sperling MR. 2019. Normal Awake, Drowsy, and Sleep EEG Patterns That
707 Might Be Overinterpreted as Abnormal. *Journal of Clinical Neurophysiology*.
708 doi:10.1097/WNP.0000000000000585
- 709 Attwell D, Buchan AM, Chrapak S, Lauritzen M, Macvicar BA, Newman EA. 2010. Glial and
710 neuronal control of brain blood flow. *Nature* **468**:232–243. doi:10.1038/nature09613
- 711 Attwell D, Mishra A, Hall CN, O’Farrell FM, Dalkara T. 2016. What is a pericyte? *Journal of*
712 *Cerebral Blood Flow and Metabolism* **36**:451–455. doi:10.1177/0271678X15610340
- 713 Baraban SC. 2004. Neuropeptide Y and epilepsy: Recent progress, prospects and
714 controversies. *Neuropeptides*. doi:10.1016/j.npep.2004.04.006
- 715 Berwick J, Johnston D, Jones M, Martindale J, Martin C, Kennerley AJ, Redgrave P, Mayhew
716 JEW. 2008. Fine detail of neurovascular coupling revealed by spatiotemporal analysis of
717 the hemodynamic response to single whisker stimulation in rat barrel cortex. *J*
718 *Neurophysiol* **99**:787–798. doi:10.1152/jn.00658.2007
- 719 Bezzina C, Verret L, Juan C, Remaud J, Halley H, Rampon C, Dahan L. 2015. Early onset of
720 hypersynchronous network activity and expression of a marker of chronic seizures in the
721 Tg2576 mouse model of Alzheimer’s disease. *PLoS One* **10**.
722 doi:10.1371/journal.pone.0119910
- 723 Blanco M, Stern JE, Filosa JA. 2008. Tone-dependent vascular responses to astrocyte-derived
724 signals. *American journal of physiology* 2855–2863. doi:10.1152/ajpheart.91451.2007.
- 725 Boie Y, Stocco R, Sawyer N, Slipetz DM, Ungrin MD, Neuschafer-rube F, Puschel GP. 1997.
726 Molecular cloning and characterization of the four rat prostaglandin E 2 prostanoid
727 receptor subtypes 227–241.
- 728 Caswell TA, Andrade ES de, Lee A, Droettboom M, Hoffmann T, Klymak J, Hunter J, Firing E,
729 Stansby D, Varoquaux N, Nielsen JH, Gustafsson O, Root B, May R, Elson P, Seppänen JK,
730 Lee J-J, Dale D, Sunden K, hannah, McDougall D, Straw A, Hobson P, Lucas G, Gohlke C,

- 731 Vincent AF, Yu TS, Ma E, Silvester S, Moad C. 2023. matplotlib/matplotlib: REL: v3.7.2.
732 doi:10.5281/ZENODO.8118151
- 733 Cauli B, Dusart I, Li D. 2023. Lactate as a determinant of neuronal excitability, neuroenergetics
734 and beyond. *Neurobiol Dis* **184**:106207. doi:10.1016/j.nbd.2023.106207
- 735 Cauli B, Hamel E. 2010. Revisiting the role of neurons in neurovascular coupling. *Front*
736 *Neuroenergetics* **2**:9. doi:10.3389/fnene.2010.00009
- 737 Cauli B, Tong XK, Rancillac A, Serluca N, Lambolez B, Rossier J, Hamel E. 2004. Cortical GABA
738 interneurons in neurovascular coupling: Relays for subcortical vasoactive pathways.
739 *Journal of Neuroscience* **24**:8940–8949. doi:10.1523/JNEUROSCI.3065-04.2004
- 740 Chaudhry UA, Zhuang H, Crain BJ, Doré S. 2008. Elevated microsomal prostaglandin-E
741 synthase-1 in Alzheimer's disease. *Alzheimer's and Dementia* **4**:6–13.
742 doi:10.1016/j.jalz.2007.10.015
- 743 Chung DY, Sadeghian H, Qin T, Lule S, Lee H, Karakaya F, Goins S, Oka F, Yaseen MA, Houben
744 T, Tolner EA, Van Den Maagdenberg AMJMJM, Whalen MJ, Sakadžić S, Ayata C. 2018.
745 Determinants of Optogenetic Cortical Spreading Depolarizations. *Cerebral Cortex* **29**:1–
746 12. doi:10.1093/cercor/bhy021
- 747 Clasadonte J, Poulain P, Hanchate NK, Corfas G, Ojeda SR, Prevot V. 2011. Prostaglandin E 2
748 release from astrocytes triggers gonadotropin-releasing hormone (GnRH) neuron firing
749 via EP2 receptor activation. *Proc Natl Acad Sci U S A* **108**:16104–16109.
750 doi:10.1073/pnas.1107533108
- 751 Dabertrand F, Hannah RM, Pearson JM, Hill-Eubanks DC, Brayden JE, Nelson MT. 2013.
752 Prostaglandin E2, a postulated astrocyte-derived neurovascular coupling agent,
753 constricts rather than dilates parenchymal arterioles. *Journal of Cerebral Blood Flow and*
754 *Metabolism* **33**:479–482. doi:10.1038/jcbfm.2013.9
- 755 Desai S, April H, Nwaneshiudu C, Ashby B. 2000. Comparison of agonist-induced internalization
756 of the human EP2 and EP4 prostaglandin receptors: Role of the carboxyl terminus in EP4
757 receptor sequestration. *Mol Pharmacol* **58**:1279–1286. doi:10.1124/mol.58.6.1279

- 758 Devienne G, Le Gac B, Piquet J, Cauli B. 2018. Single Cell Multiplex Reverse Transcription
759 Polymerase Chain Reaction After Patch-Clamp. *Journal of Visualized Experiments* **136**:1–
760 12. doi:10.3791/57627
- 761 Devor A, Hillman EMC, Tian P, Waeber C, Teng IC, Ruvinskaya L, Shalinsky MH, Zhu H, Haslinger
762 RH, Narayanan SN, Ulbert I, Dunn AK, Lo EH, Rosen BR, Dale AM, Kleinfeld D, Boas DA.
763 2008. Stimulus-Induced Changes in Blood Flow and 2-Deoxyglucose Uptake Dissociate in
764 Ipsilateral Somatosensory Cortex. *Journal of Neuroscience* **28**:14347–14357.
765 doi:10.1523/JNEUROSCI.4307-08.2008
- 766 Devor A, Tian P, Nishimura N, Teng IC, Hillman EMC, Narayanan SN, Ulbert I, Boas DA, Kleinfeld
767 D, Dale AM. 2007. Suppressed Neuronal Activity and Concurrent Arteriolar
768 Vasoconstriction May Explain Negative Blood Oxygenation Level-Dependent Signal.
769 *Journal of Neuroscience* **27**:4452–4459. doi:10.1523/JNEUROSCI.0134-07.2007
- 770 Di Cesare A, Del Piccolo P, Zacchetti D, Grohovaz F. 2006. EP2 receptor stimulation promotes
771 calcium responses in astrocytes via activation of the adenylyl cyclase pathway. *Cellular
772 and Molecular Life Sciences* **63**:2546–2553. doi:10.1007/s00018-006-6262-9
- 773 Farrell JS, Gaxiola-Valdez I, Wolff MD, David LS, Dika HI, Geeraert BL, Wang R, Singh S,
774 Spanswick SC, Dunn JF, Antle MC, Federico P, Campbell Teskey G. 2016. Postictal
775 behavioural impairments are due to a severe prolonged hypoperfusion/ hypoxia event
776 that is COX-2 dependent. doi:10.7554/eLife.19352.001
- 777 Gheres KW, Ünsal HS, Han X, Zhang Q, Turner KL, Zhang N, Drew PJ. 2023. Arousal state
778 transitions occlude sensory-evoked neurovascular coupling in neonatal mice. *Commun
779 Biol* **6**. doi:10.1038/s42003-023-05121-5
- 780 Gicquiaux H, Lecat S, Gaire M, Dieterlen A, Mély Y, Takeda K, Bucher B, Galzi JL. 2003.
781 Neuropeptide Y-induced contraction and its desensitization through the neuropeptide Y
782 receptor subtype in several rat veins. *J Cardiovasc Pharmacol* **41 Suppl 1**:S23-7.
- 783 Gicquiaux H, Lecat S, Gaire M, Dieterlen A, Mély Y, Takeda K, Bucher B, Galzi JL. 2002. Rapid
784 internalization and recycling of the human neuropeptide Y Y1 receptor. *Journal of
785 Biological Chemistry* **277**:6645–6655. doi:10.1074/jbc.M107224200

- 786 Girouard H, Bonev AD, Hannah RM, Meredith A, Aldrich RW, Nelson MT. 2010. Astrocytic
787 endfoot Ca²⁺ and BK channels determine both arteriolar dilation and constriction. *Proc*
788 *Natl Acad Sci U S A* **107**:3811–3816. doi:10.1073/pnas.0914722107
- 789 Gordon GRJ, Choi HB, Rungta RL, Ellis-Davies GCR, MacVicar BA. 2008. Brain metabolism
790 dictates the polarity of astrocyte control over arterioles. *Nature* **456**:745–9.
791 doi:10.1038/nature07525
- 792 Gorski JA, Talley T, Qiu M, Puelles L, Rubenstein JLRR, Jones KR. 2002. Cortical excitatory
793 neurons and glia, but not GABAergic neurons, are produced in the Emx1-expressing
794 lineage. *Journal of Neuroscience* **22**:6309–6314. doi:10.1523/jneurosci.22-15-
795 06309.2002
- 796 Grutzendler J, Nedergaard M. 2019. Cellular Control of Brain Capillary Blood Flow: In Vivo
797 Imaging Veritas. *Trends Neurosci*. doi:10.1016/j.tins.2019.05.009
- 798 Hartmann DA, Berthiaume AA, Grant RI, Harrill SA, Koski T, Tieu T, McDowell KP, Faino A V.,
799 Kelly AL, Shih AY. 2021. Brain capillary pericytes exert a substantial but slow influence on
800 blood flow. *Nat Neurosci* **24**:633–645. doi:10.1038/s41593-020-00793-2
- 801 Hill RA, Tong L, Yuan P, Murikinati S, Gupta S, Grutzendler J. 2015. Regional Blood Flow in the
802 Normal and Ischemic Brain Is Controlled by Arteriolar Smooth Muscle Cell Contractility
803 and Not by Capillary Pericytes. *Neuron* **87**:95–110. doi:10.1016/j.neuron.2015.06.001
- 804 Iadecola C. 2017. The Neurovascular Unit Coming of Age: A Journey through Neurovascular
805 Coupling in Health and Disease. *Neuron* **96**:17–42. doi:10.1016/j.neuron.2017.07.030
- 806 Iadecola C, Nedergaard M. 2007. Glial regulation of the cerebral microvasculature. *Nat*
807 *Neurosci* **10**:1369–1376. doi:10.1038/nn2003
- 808 Jiruska P, de Curtis M, Jefferys JGR, Schevon CA, Schiff SJ, Schindler K. 2013. Synchronization
809 and desynchronization in epilepsy: Controversies and hypotheses. *Journal of Physiology*.
810 doi:10.1113/jphysiol.2012.239590
- 811 Kahn I, Knoblich U, Desai M, Bernstein J, Graybiel AM, Boyden ES, Buckner RL, Moore CI. 2013.
812 Optogenetic drive of neocortical pyramidal neurons generates fMRI signals that are

- 813 correlated with spiking activity. *Brain Res* **1511**:33–45.
814 doi:10.1016/j.brainres.2013.03.011
- 815 Karagiannis A, Gallopin T, Dávid C, Battaglia D, Geoffroy H, Rossier J, Hillman EMC, Staiger JF,
816 Cauli B. 2009. Classification of NPY-expressing neocortical interneurons. *J Neurosci*
817 **29**:3642–59. doi:10.1523/JNEUROSCI.0058-09.2009
- 818 Karagiannis A, Gallopin T, Lacroix A, Plaisier F, Piquet J, Geoffroy H, Hepp R, Naudé J, Le Gac B,
819 Egger R, Lambolez B, Li D, Rossier J, Staiger JF, Imamura H, Seino S, Roeper J, Cauli B.
820 2021. Lactate is an energy substrate for rodent cortical neurons and enhances their firing
821 activity. *Elife* **10**:1–40. doi:10.7554/elife.71424
- 822 Kasischke KA, Lambert EM, Panepento B, Sun A, Gelbard HA, Burgess RW, Foster TH,
823 Nedergaard M. 2011. Two-photon NADH imaging exposes boundaries of oxygen diffusion
824 in cortical vascular supply regions. *Journal of Cerebral Blood Flow and Metabolism* **31**:68–
825 81. doi:10.1038/jcbfm.2010.158
- 826 Krawchuk MB, Ruff CF, Yang X, Ross SE, Vazquez AL. 2020. Optogenetic assessment of VIP, PV,
827 SOM and NOS inhibitory neuron activity and cerebral blood flow regulation in mouse
828 somato-sensory cortex. *Journal of Cerebral Blood Flow and Metabolism* **40**:1427–1440.
829 doi:10.1177/0271678X19870105
- 830 Lacroix A, Toussay X, Anenberg E, Lecrux C, Ferreirós N, Karagiannis A, Plaisier F, Chausson P,
831 Jarlier F, Burgess SA, Hillman EMCCC, Tegeder I, Murphy TH, Hamel E, Cauli B, Ferreiro N,
832 Burgess SA, Hillman EMCCC, Tegeder I, Murphy TH, Hamel E, Cauli B. 2015. COX-2-
833 Derived Prostaglandin E2 Produced by Pyramidal Neurons Contributes to Neurovascular
834 Coupling in the Rodent Cerebral Cortex. *J Neurosci* **35**:11791–11810.
835 doi:10.1523/JNEUROSCI.0651-15.2015
- 836 Lecrux C, Toussay X, Kocharyan A, Fernandes P, Neupane S, Levesque M, Plaisier F, Shmuel A,
837 Cauli B, Hamel E. 2011. Pyramidal Neurons Are “Neurogenic Hubs” in the Neurovascular
838 Coupling Response to Whisker Stimulation. *Journal of Neuroscience* **31**:9836–9847.
839 doi:10.1523/JNEUROSCI.4943-10.2011
- 840 Lee JM, Stile CL, Bice AR, Rosenthal ZP, Yan P, Snyder AZ, Lee JM, Bauer AQ. 2020. Opposed
841 hemodynamic responses following increased excitation and parvalbumin-based

- 842 inhibition. *Journal of Cerebral Blood Flow and Metabolism*.
843 doi:10.1177/0271678X20930831
- 844 Lin JY, Lin MZ, Steinbach P, Tsien RY. 2009. Characterization of engineered channelrhodopsin
845 variants with improved properties and kinetics. *Biophys J* **96**:1803–1814.
846 doi:10.1016/j.bpj.2008.11.034
- 847 Ma Y, Shaik MA, Kozberg MG, Kim SH, Portes JP, Timerman D. 2016. Resting-state
848 hemodynamics are spatiotemporally coupled to synchronized and symmetric neural
849 activity in excitatory neurons. *Proceedings of the National Academy of Sciences*.
850 doi:10.1073/pnas.1525369113
- 851 Madisen L, Mao T, Koch H, Zhuo J, Berenyi A, Fujisawa S, Hsu Y-W a, Garcia AJ, Gu X, Zanella
852 S, Kidney J, Gu H, Mao Y, Hooks BM, Boyden ES, Buzsáki G, Ramirez JM, Jones AR, Svoboda
853 K, Han X, Turner EE, Zeng H. 2012. A toolbox of Cre-dependent optogenetic transgenic
854 mice for light-induced activation and silencing. *Nat Neurosci* **15**:793–802.
855 doi:10.1038/nn.3078
- 856 Meurs A, Portelli J, Clinckers R, Balasubramaniam A, Michotte Y, Smolders I. 2012.
857 Neuropeptide Y increases in vivo hippocampal extracellular glutamate levels through Y1
858 receptor activation. *Neurosci Lett* **510**:143–147. doi:10.1016/j.neulet.2012.01.023
- 859 Mishra A, Reynolds JP, Chen Y, Gourine A V., Rusakov DA, Attwell D. 2016. Astrocytes mediate
860 neurovascular signaling to capillary pericytes but not to arterioles. *Nat Neurosci* **19**:1619–
861 1627. doi:10.1038/nn.4428
- 862 Mulligan SJ, MacVicar BA. 2004. Calcium transients in astrocyte endfeet cause cerebrovascular
863 constrictions. *Nature* **431**:195–199. doi:10.1038/nature02827
- 864 Niwa K, Araki E, Morham SG, Ross ME, Iadecola C. 2000. Cyclooxygenase-2 contributes to
865 functional hyperemia in whisker-barrel cortex. *Journal of Neuroscience* **20**:763–770.
866 doi:10.1523/jneurosci.20-02-00763.2000
- 867 O’Herron P, Chhatbar PY, Levy M, Shen Z, Schramm AE, Lu Z, Kara P. 2016. Neural correlates
868 of single-vessel haemodynamic responses in vivo. *Nature* **534**:378–382.
869 doi:10.1038/nature17965

- 870 Palop JJ, Chin J, Roberson ED, Wang J, Thwin MT, Bien-Ly N, Yoo J, Ho KO, Yu GQ, Kreitzer A,
871 Finkbeiner S, Noebels JL, Mucke L. 2007. Aberrant Excitatory Neuronal Activity and
872 Compensatory Remodeling of Inhibitory Hippocampal Circuits in Mouse Models of
873 Alzheimer's Disease. *Neuron* **55**:697–711. doi:10.1016/j.neuron.2007.07.025
- 874 Palop JJ, Mucke L. 2010. Amyloid-B-induced neuronal dysfunction in Alzheimer's disease:
875 From synapses toward neural networks. *Nat Neurosci* **13**:812–818. doi:10.1038/nn.2583
- 876 Pasinetti GM, Aisen PS. 1998. Cyclooxygenase-2 expression is increased in frontal cortex of
877 Alzheimer's disease brain. *Neuroscience* **87**:319–324. doi:10.1016/S0306-
878 4522(98)00218-8
- 879 Pellerin L, Magistretti PJ. 1994. Glutamate uptake into astrocytes stimulates aerobic glycolysis:
880 A mechanism coupling neuronal activity to glucose utilization. *Proc Natl Acad Sci U S A*
881 **91**:10625–10629. doi:10.1073/pnas.91.22.10625
- 882 Pham C, Komaki Y, Deàs-Just A, Le Gac B, Mouffle C, Franco C, Chaperon A, Vialou V,
883 Tsurugizawa T, Cauli B, Li D. 2024. Astrocyte aquaporin mediates a tonic water efflux
884 maintaining brain homeostasis. *Elife* **13**. doi:10.7554/eLife.95873
- 885 Rancillac A, Rossier J, Guille M, Tong X-K, Geoffroy H, Amatore C, Arbault S, Hamel E, Cauli B.
886 2006. Glutamatergic Control of Microvascular Tone by Distinct GABA Neurons in the
887 Cerebellum. *J Neurosci* **26**:6997–7006. doi:10.1523/JNEUROSCI.5515-05.2006
- 888 Rosehart AC, Longden TA, Weir N, Fontaine JT, Joutel A, Dabertrand F. 2021. Prostaglandin E2
889 Dilates Intracerebral Arterioles When Applied to Capillaries: Implications for Small Vessel
890 Diseases. *Front Aging Neurosci* **13**:1–11. doi:10.3389/fnagi.2021.695965
- 891 Rungta RL, Chaigneau E, Osmanski BF, Charpak S. 2018. Vascular Compartmentalization of
892 Functional Hyperemia from the Synapse to the Pia. *Neuron* 1–14.
893 doi:10.1016/j.neuron.2018.06.012
- 894 Rungta RL, Osmanski B-F, Boido D, Tanter M, Charpak S. 2017. Light controls cerebral blood
895 flow in naive animals. *Nat Commun* **8**:14191. doi:10.1038/ncomms14191
- 896 Rungta RL, Zuend M, Aydin A, Weber B, Charpak S, Boido D. 2021. vascular arbors in layer II /
897 III somatosensory cortex. *Commun Biol*. doi:10.1038/s42003-021-02382-w

- 898 Sada N, Lee S, Katsu T, Otsuki T, Inoue T. 2015. Targeting LDH enzymes with a stiripentol analog
899 to treat epilepsy. *Science (1979)* **347**:1362–1367. doi:10.1126/science.aaa1299
- 900 Sang N, Zhang J, Marcheselli V, Bazan NG, Chen C. 2005. Postsynaptically Synthesized
901 Prostaglandin E2 (PGE2) Modulates Hippocampal Synaptic Transmission via a Presynaptic
902 PGE2 EP2 Receptor. *Journal of Neuroscience* **25**:9858–9870.
903 doi:10.1523/JNEUROSCI.2392-05.2005
- 904 Schmid F, Barrett MJPP, Jenny P, Weber B. 2019. Vascular density and distribution in
905 neocortex. *Neuroimage* **197**:792–805. doi:10.1016/j.neuroimage.2017.06.046
- 906 Scott NA, Murphy TH. 2012. Hemodynamic responses evoked by neuronal stimulation via
907 channelrhodopsin-2 can be independent of intracortical glutamatergic synaptic
908 transmission. *PLoS One* **7**:1–10. doi:10.1371/journal.pone.0029859
- 909 Sharif NA, Klimko PG. 2019. Prostaglandin FP receptor antagonists: discovery, pharmacological
910 characterization and therapeutic utility. *Br J Pharmacol* **176**:1059–1078.
911 doi:10.1111/bph.14335
- 912 Shmuel A, Yacoub E, Pfeuffer J, Moortele P Van De, Adriany G, Hu X, Ugurbil K, Van de
913 Moortele PF, Adriany G, Hu X, Ugurbil K. 2002. Sustained negative BOLD, blood flow and
914 oxygen consumption response and its coupling to the positive response in the human
915 brain. *Neuron* **36**:1195–1210. doi:10.1016/S0896-6273(02)01061-9
- 916 Smetters D, Majewska A, Yuste R. 1999. Detecting action potentials in neuronal populations
917 with calcium imaging. *Methods: A Companion to Methods in Enzymology* **18**:215–221.
918 doi:10.1006/meth.1999.0774
- 919 Smith SJ, Smbül U, Graybuck LT, Collman F, Seshamani S, Gala R, Gliko O, Elabbady L, Miller
920 JA, Bakken TE, Rossier J, Yao Z, Lein E, Zeng H, Tasic B, Hawrylycz M. 2019. Single-cell
921 transcriptomic evidence for dense intracortical neuropeptide networks. *Elife* **8**:1–35.
922 doi:10.7554/eLife.47889
- 923 Sun W, McConnell E, Pare J-F, Xu Q, Chen M, Peng W, Lovatt D, Han X, Smith Y, Nedergaard
924 M. 2013. Glutamate-Dependent Neuroglial Calcium Signaling Differs Between Young and
925 Adult Brain. *Science (1979)* **339**:197–200. doi:10.1126/science.1226740

- 926 Takei S, Hasegawa-Ishii S, Uekawa A, Chiba Y, Umegaki H, Hosokawa M, Woodward DF,
927 Watanabe K, Shimada A. 2012. Immunohistochemical demonstration of increased
928 prostaglandin F2 α levels in the rat hippocampus following kainic acid-induced seizures.
929 *Neuroscience* **218**:295–304. doi:10.1016/j.neuroscience.2012.05.013
- 930 Takemiya T, Matsumura K, Yamagata K. 2007. Roles of prostaglandin synthesis in excitotoxic
931 brain diseases. *Neurochem Int* **51**:112–120. doi:10.1016/j.neuint.2007.05.009
- 932 Tasic B, Menon V, Nguyen TNTN, Kim TKTKTK, Jarsky T, Yao Z, Levi BBP, Gray LT, Sorensen SA,
933 Dolbear T, Bertagnolli D, Goldy J, Shapovalova N, Parry S, Lee CCK, Smith K, Bernard A,
934 Madisen L, Sunkin SM, Hawrylycz M, Koch C, Zeng H, Yao Z, Lee CCK, Shapovalova N, Parry
935 S, Madisen L, Sunkin SM, Hawrylycz M, Koch C, Zeng H. 2016. Adult mouse cortical cell
936 taxonomy revealed by single cell transcriptomics. *Nat Neurosci advance on*:1–37.
937 doi:10.1038/nn.4216
- 938 Team RC, R Core Team, Team RC. 2023. R: A Language and Environment for Statistical
939 Computing.
- 940 Thévenaz P, Ruttimann UE, Unser M. 1998. A pyramid approach to subpixel registration based
941 on intensity. *IEEE Transactions on Image Processing* **7**:27–41. doi:10.1109/83.650848
- 942 Tournissac M, Boido D, Omnès M, Goulam-Houssen Y, Ciobanu L, Charpak S. 2022. Cranial
943 window for longitudinal and multimodal imaging of the whole mouse cortex.
944 *Neurophotonics* **9**. doi:10.1117/1.nph.9.3.031921
- 945 Tran CHT, George AG, Teskey GC, Gordon GR. 2020. Seizures elevate gliovascular unit Ca²⁺
946 and cause sustained vasoconstriction. *JCI Insight* **5**. doi:10.1172/jci.insight.136469
- 947 Tsai CJ, Nagata T, Liu CY, Suganuma T, Kanda T, Miyazaki T, Liu K, Saitoh T, Nagase H, Lazarus
948 M, Vogt KE, Yanagisawa M, Hayashi Y. 2021. Cerebral capillary blood flow upsurge during
949 REM sleep is mediated by A2a receptors. *Cell Rep* **36**. doi:10.1016/j.celrep.2021.109558
- 950 Tsurumaki T, Yamaguchi T, Higuchi H. 2002. Marked neuropeptide Y-induced contractions via
951 NPY-Y1 receptor and its desensitization in rat veins. *Vascul Pharmacol* **39**:325–333.
952 doi:10.1016/S1537-1891(03)00044-2

- 953 Uhlirova H, Kılıç K, Tian P, Thunemann M, Desjardins M, Saisan PA, Sakadžić S, Ness T V., Mateo
954 C, Cheng Q, Weldy KL, Razoux F, Vandenberghe M, Cremonesi JA, Ferri CGL, Nizar K,
955 Sridhar VB, Steed TC, Abashin M, Fainman Y, Masliah E, Djurovic S, Andreassen OA, Silva
956 GA, Boas DA, Kleinfeld D, Buxton RB, Einevol GT, Dale AM, Devor A, Kilic K, Tian P,
957 Thunemann M, Ness T V., Saisan PA, Sakadz S, Mateo C, Cheng Q, Weldy KL, Razoux F,
958 Vandenberghe M, Cremonesi JA, Ferri CGL, Nizar K, Sridhar VB, Steed TC, Abashin M, Silva
959 GA, Boas DA, Kleinfeld D, Buxton RB. 2016. Cell type specificity of neurovascular coupling
960 in cerebral cortex. *Elife* **5**:1–23. doi:10.7554/eLife.14315
- 961 Voutsinos-Porche B, Bonvento G, Tanaka K, Steiner P, Welker E, Chatton JY, Magistretti PJ,
962 Pellerin L. 2003. Glial glutamate transporters mediate a functional metabolic crosstalk
963 between neurons and astrocytes in the mouse developing cortex. *Neuron* **37**:275–286.
964 doi:10.1016/S0896-6273(02)01170-4
- 965 Wagner L, Wolf R, Zeitschel U, Rossner S, Petersén Å, Leavitt BR, Kästner F, Rothermundt M,
966 Gärtner UT, Gündel D, Schlenzig D, Frerker N, Schade J, Manhart S, Rahfeld JU, Demuth
967 HU, Von Hörsten S. 2015. Proteolytic degradation of neuropeptide γ (NPY) from head to
968 toe: Identification of novel NPY-cleaving peptidases and potential drug interactions in
969 CNS and Periphery. *J Neurochem* **135**:1019–1037. doi:10.1111/jnc.13378
- 970 Yamagata K, Andreasson KI, Kaufmann WE, Barnes CA, Worley PF. 1993. Expression of a
971 Mitogen-Inducible Cyclooxygenase in Brain Neurons : Regulation by Synaptic Activity and
972 Glucocorticoids. *Neuron* **11**:371–386. doi:10.1016/0896-6273(93)90192-t
- 973 Yamagata K, Matsumura K, Inoue W, Shiraki T, Suzuki K, Yasuda S, Sugiura H, Cao C, Watanabe
974 Y, Kobayashi S. 2001. Coexpression of microsomal-type prostaglandin E synthase with
975 cyclooxygenase-2 in brain endothelial cells of rats during endotoxin-induced fever.
976 *Journal of Neuroscience* **21**:2669–2677. doi:10.1523/jneurosci.21-08-02669.2001
- 977 Zeisel A, Muñoz-Manchado AB, Codeluppi S, Lönnerberg P, La Manno G, Juréus A, Marques S,
978 Munguba H, He L, Betsholtz C, Rolny C, Castelo-Branco G, Hjerling-Leffler J, Linnarsson S.
979 2015. Cell types in the mouse cortex and hippocampus revealed by single-cell RNA-seq.
980 *Science (1979)* **347**:1138–1142.
- 981 Zhang D, Ruan J, Peng S, Li J, Hu X, Zhang Y, Zhang T, Ge Y, Zhu Z, Xiao X, Zhu YY, Li XX, Li T,
982 Zhou L, Gao Q, Zheng G, Zhao B, Li XX, Zhu YY, Wu J, Li W, Zhao J, Ge W, Xu T, Jia J-M.

- 983 2024. Synaptic-like transmission between neural axons and arteriolar smooth muscle
984 cells drives cerebral neurovascular coupling. *Nat Neurosci* 1–17. doi:10.1038/s41593-
985 023-01515-0
- 986 Zhang DY, Raichle ME. 2010. Disease and the brain’s dark energy. *Nat Rev Neurol* 6:15–28.
987 doi:10.1038/nrneurol.2009.198
- 988 Zhou N, Gordon GRJ, Feighan D, MacVicar BA. 2010. Transient swelling, acidification, and
989 mitochondrial depolarization occurs in neurons but not astrocytes during spreading
990 depression. *Cerebral Cortex* 20:2614–2624. doi:10.1093/cercor/bhq018
- 991 Zonta M, Angulo MC, Gobbo S, Rosengarten B, Hossmann K-A, Pozzan T, Carmignoto G. 2003.
992 Neuron-to-astrocyte signaling is central to the dynamic control of brain microcirculation.
993 *Nat Neurosci* 6:43–50. doi:10.1038/nn980

